VOLUME 19 NO. 2 | JULY 2025
P-ISSN: 1411-1616 | E-ISSN:2549-8215

JURNAL ILMIAH BERKALA
SAINS DAN TERAPAN KIMIA

Silica extraction results from Sinabung volcanic ash (Malau *et al*, p. 29)

JURNAL ILMIAH BERKALA
SAINS DAN TERAPAN
KIMIA

PUBLISHED BY:
CHEMISTRY DEPARTMENT, FACULTY OF MATHEMATICS AND NATURAL SCIENCES
LAMBUNG MANGKURAT UNIVERSITY, INDONESIA

SUPERVISORY BOARD

Head of Chemistry Department, Faculty of Mathematics and Natural Sciences, Lambung Mangkurat University

PUBLISHER

Chemistry Department, Faculty of Mathematics and Natural Sciences, Lambung Mangkurat University

MAILING ADDRESS

Jl. A. Yani Km. 36 Banjarbaru, Kalimantan Selatan , Indonesia 70714
Phone: 0511-4773112, 0511-4782899
Email: jstk@ulm.ac.id

FIRST EDITION: 2007

EDITOR IN CHIEF

Dahlena Ariyani, S.Si., M.S.

EDITORIAL BOARD

Associate Editors : Dyah Ayu Pramoda Wardani, M.Sc.
Section Editors : Achmad Ramadhanna'il Rasjava, S.Si., M.Si.

Editorial Board Members:

Prof. Dr. Abdullah, S.Si, M.Si (Universitas Lambung Mangkurat, Banjarbaru)
Prof. Dr. Gusrizal, S.Si., M.Si. (Universitas Tanjungpura, Pontianak)
Prof. Dr. Rer.nat Drs. Karna Wijaya, M.Eng (UGM, Yogyakarta)
Prof. Sunardi, S.Si., M.Sc., Ph.D. (Universitas Lambung Mangkurat, Banjarbaru)
Dr. RR. Dirgarini Julia Nurlianti Subagyono (Universitas Mulawarman, Samarinda)
Sura Menda Ginting, Ph.D. (Universitas Bengkulu, Bengkulu)
Yuana Nurulita,S.Si, M.Si, Ph.D (Universitas Riau, Riau)
Achmad Ramadhanna'il Rasjava, S.Si., M.Si. (Universitas Lambung Mangkurat)
Dahlena Ariyani, S.Si., M.S. (Universitas Lambung Mangkurat)
Dyah Ayu Pramoda Wardani, M.Sc. (Universitas Lambung Mangkurat)

SITE EDITOR AND ADMINISTRATOR

Dyah Ayu Pramoda Wardani, M.Sc.
Achmad Ramadhanna'il Rasjava, S.Si., M.Si.
Aulia Rhamdani Arfan, S.Si., M.Si.

ABOUT US

(Jurnal Ilmiah Berkala) Sains dan Terapan Kimia publishes scientific articles in the Chemistry field which include, but not limited to, research in chemistry, theoretical chemistry, and applied chemistry. This journal also publishes review articles about the development of chemistry. All the articles in this journal will go through a peer-review process to ensure that the quality of the article meets our standard before being published. Each article submitted to our journal will be reviewed by a reviewer having the expertise in the field. Shall the article submitted is deemed acceptable to be published in our journal, it is the writer's responsibility to make the necessary change and revision as recommended by the reviewer.
This journal is open access journal which means that all content is freely available without charge to users or / institution. Users are allowed to read, download, copy, distribute, print, search, or link to full text articles in this journal without asking prior permission from the publisher or author.

Sains dan Terapan Kimia (Jurnal Ilmiah Berkala) is published twice a year on January and July. There is no fee for authors to submit their manuscripts to be considered for publication in this jurnal. When the article is accepted for the publication. The publication fee is IDR 350.000,00 that covers article processing and DOI processing charge. Payment should be made by bank transfer to this account below

Bank	: BNI Banjarbaru
Account Number	**107840008**
Account Name	: Dahlena Ariyani

Please send a confirmation of your proof of payment to jstk@ulm.ac.id

TABLE OF CONTENTS

Valorization of Peanut Shell (*Arachis hypogeae*) Composited Humic Acid as Bioadsorbent of Heavy Metal Contamination.....1-12
Ninik Triayu Susparini*, Muksin, Marwita, Adfin Afriyandi, Fahri Rozanno Putra

Larvacidal And *Oviposition Deterrent* Activity of Dragon Scale Fern (*Pyrrosia piloselloides* (L.) M. G. Price) Extract Against *Culex sp*……..... 13-25
Khodijah Amini Tanjung, Halimatussakdiah Halimatussakdiah*, and Muslimah Muslimah

Fluorescent Silica Nanofertilizer for Enhancement of Photosynthesis Rate.....26-34
Fransiskus Hottua Malau, Carlos Rewandesno Sitorus, Pebry Asarona Sianipar, Winri Imanuela Sihombing, Nurul Pratiwi Santoso, Lisnawaty Simatupang*

Photocatalytic Degradation of Phenol Red Using Titanium Dioxide (TiO_2)–Chitosan Composite Catalyst Assisted By Solar Energy.....35-43
M. Ridwan Baidhowi*, Taufiqur Rohman, Utami Irawati

Study on the Effect of Chitosan Concentration on the Synthesis of Epichlorohydrin Crosslinked Charcoal-Chitosan Composite on Its Ability To Adsorb Naphthol Blue Black Dye..... 44-56
Salma Nur Aida, Dahlena Ariyani* Umi Baroroh Lili Utami, Dyah Ayu Pramoda Wardani, Ahmad Budi Junaidi [1)]

JURNAL ILMIAH BERKALA SAINS DAN TERAPAN KIMIA

Jurnal Ilmiah Berkala: Sains dan Terapan Kimia
Vol. 19 No. 2, Juli 2025

Valorization of Peanut Shell (*Arachis hypogeae*) Composited Humic Acid as Bioadsorbent of Heavy Metal Contamination

Valorisasi Limbah Kulit Kacang Tanah (*Arachis hypogeae*) Terkomposit Asam Humat sebagai Bioadsorben Cemaran Logam Berat

Ninik Triayu Susparini*, Muksin, Marwita, Adfin Afriyandi, Fahri Rozanno Putra

Department of Chemical Analyst, Sekolah Tinggi Analis Kimia Cilegon, South Ring Road KM 17 Harjatani, Serang, 42161, Indonesia

Email: *niniktriayu@gmail.com*

ABSTRACT

The problem of organic and industrial waste still be the focus problems in Indonesia, especially in Cilegon city. In this research, organic waste and peanut shells were valorized into composite biosorbent to treat heavy metal contamination. The aim of this research was to create a biosorbent composite that is applied to adsorb heavy metals in industrial waste. The composite bioadsorbent was used as a source of functional groups such as –COOH and -OH phenolics and –OH alcoholates that can absorb the heavy metals. The adsorption process was carried out by mixing the biosorbent with the metal sample solution for 2h. Characterization was carried out using Fourier Transform Infrared Spectroscopy (FTIR), X-Ray Difraction (XRD), Inductively Coupled Plasma (ICP) and Scanning Electron Microscopy-Energy Dispersive X-ray (SEM-EDX). Based on the experimental results, the composite bioadsorbent had macro-sized pores which were efficient in adsorbing Pb, Al, and Fe adsorption efficiencies of 66.50%, 36.16%, and 50.96% respectively. The developed composite bioadsorbent has good application prospects in sustainable environmental processing.

Keywords: Biosorbent; Environment; Heavy Metals; Organic Waste; Peanut Shells.

Received: 17 May 2025 ; **Accepted**: 26 July 2025: **Available online**: 30 July 2025

1. INTRODUCTION

The Cilegon city, which is located in Banten Province, is one of the industrial centers in Indonesia. The waste from several industrial sectors in Cilegon, including the petrochemical and steel coating industries, is highly contaminated with heavy metals, including arsenic (As), chromium (Cr), copper (Cu), lead (Pb), mercury (Hg), and cadmium (Cd). Based on data from the Public Disclosure for Environmental Compliance (PROPER) of the Ministry of the Environment of the Republic of Indonesia in 2022, there are 21.35% of industries in Cilegon and its surroundings in the red ranking position out of a total of 103 industries [1]. So, Industrial waste that is not properly treated will cause serious environmental problems, especially waste containing heavy metals because they

are carcinogenic and difficult to degrade in the environment [2].

One way to address pollution originating from industrial waste is through adsorption methods using natural materials, commonly referred to as biosorbents [3]. Peanuts are an abundant agricultural commodity in Cilegon. Based on data from the Banten Province Central Statistics Agency in 2021 [4], peanut production reached 4054 tons, but only the seeds were used, while the shells were discarded as agricultural waste. The high cellulose content in peanut shells can be used as a natural source for producing activated carbon for biosorbent. However, the use of activated carbon as an adsorbent heavily depends on its porosity, so other materials are needed to increase binding affinity. In this study, we chose humic acid as an environmentally friendly composite material. humic acid has functional groups such as –COOH, -OH phenolates and –OH alcoholates which will experience deprotonation at alkaline pH and are able to chelate metal. The presence of this group allows humic acid to form stable complexes with heavy metal ions [5,6]. Humic acid is obtained from compost extracts made from organic waste such as vegetables obtained from traditional markets in Cilegon. This is done simultaneously to reduce the accumulation of untreated domestic waste.

Activated carbon has good stability as an adsorbent, while humic acid has a high adsorption capacity [7], so this research focuses on the use of peanut shell activated carbon composited with humic acid from organic waste extract to increase stability and efficiency of metals by the biosorbent composite chelation of metal ions. Some existing research on humic acid focuses on its function as fertilizer and plant fertilizer [8, 9, 10]. Other research on increasing the adsorption capacity of activated carbon was only carried out using the activation method [11,12,13]. Research using peanut shells as an active carbon absorbent has been studied, but there has been no research combining them with humic acid as a biosorbent. While several studies have used carbon in the form of multiwalled carbon nanotubes or graphene, this study focuses on turning organic waste, specifically, peanut shells and organic waste which are an issue in the city of Cilegon into useful materials. It is hoped that using waste-based biomaterials to deal with heavy metal contamination from industrial waste can become a strategic environmental control effort.

2. MATERIALS AND METHODS

2.1. Materials

The tools used in this research are centrifuges, ovens, analytical instruments consisting of a Fourier Transform Infrared (FTIR) Spectrophotometer, X-ray Ray Diffraction (XRD), Scanning Electron Microscope-Energy Dispersive X-Ray (SEM-EDX), Inductively Coupled Plasma (ICP), and a set of glassware. The materials used in this research where organic waste was obtained from Kranggot market, with the selected waste consisting of vegetable residues, peanut shell waste was obtained from the Mancak area, horse dung was obtained from the Gegeneng area. All samples were sourced from the Cilegon city region. Phosphoric acid, NaOH, HCl 37%, HF, standard humic acid, $Pb(NO_3)_2$, $FeSO_4.7H_2O$, and $Al_2(SO_4)_3.7H_2O$. All the methods following by Chkraborty, et al. (2020); H. Li et al. (2021); Z. Li et al. (2020) and Zingaretti et al. (2020) modified procedure and by our experimental methods.

2.2. Peanut Shell Activated Carbon Preparation

Peanut shells are washed and dried for 12 hours in the sun. Once dry, the peanut shells are roasted until they become charcoal and then crushed. The finely ground peanut shell charcoal was sieved using a 100-mesh sieve and soaked for 7 hours in a 10% H_3PO_4 solution. The soaked samples were then filtered using Whatman 42 paper and dried in an oven at 105˚C until a constant weight was reached. The activated carbon (AC) that has been produced is then neutralized with distilled water to pH 7. After being dried in an oven at 110˚C, the neutral activated carbon is examined for water content and iodine absorption capability to assess its adsorbent quality. To describe functional group in

activated carbon, used Fourier transform infrared spectroscopy (FTIR).

2.3. Compost Production

The production of compost from organic waste aims to serve as the primary material for generating humic acid. Organic waste obtained from Kranggot Market, Cilegon-Banten, is mixed with dried horse manure as a starter in a ratio of 2:1. The mixture is anaerobically placed in a 20 L composting tank. The compost is irrigated once a week using 500 mL of EM4 and a sugar solution. The composting process takes place for around one month. After one month, the compost was dried naturally in the sun for 2 days. Drying continued in an oven for 36 hours. The dry compost is then crushed and uniform in size using a 100-mesh sieve.

2.4. Humic Acid Extraction

A total of 250 g of dry compost was added to 3 L of 0.1 M NaOH solution and shaken for 2 hours, then left for 24 hours. The next day, the liquid was centrifuged at 3950 rpm for 15 minutes. Filter the filtrate and acidify with concentrated HCl, shake for 2 hours and leave for 24 hours. The crude extract was centrifuged at 3950 rpm for 15 minutes, and then the sediment was separated from the filtrate. The precipitation obtained is crude humic acid. Crude humic acid was purified with a solution of 0.1 M Hydrochloric Acid (HCl) and 0.3 M Hydrofluoric Acid HF at 1:1 four times. The purification results are then washed with distilled water. Pure humic acid was then oven-treated at 40 °C and characterized by Fourier Transform Infrared Spectroscopy (FTIR) and X-ray Diffraction (XRD).

2.5. Synthesis Activated Carbon Composites - Humic Acid

Synthesis of activated carbon composite with humic acid aimed at a high metal adsorption capacity biosorbent. The solution containing 0.3 g humic acid in 50 mL of distilled water was stirred with a magnetic stirrer for 6 hours to obtain a saturated solution. Then it was filtered using Whatman 42 filter paper, followed by the addition of 50 mL of the mixture containing 0.5 g activated carbon adjusted to pH 8.5 with a 0.1 M Tris buffer solution. The resulting mixture was stirred for 12 hours with a magnetic stirrer and then filtered. The filtered result obtained is called a biosorbent composite. The biosorbent composite formed was washed three times with distilled water and dried at 60 °C for 24 hours.

2.6. Batch Adsorption of Heavy Metals and Real Sample Applications

A mixture of the heavy metals Pb, Al, and Fe from the salts of $Pb(NO_3)_2$, $Al_2(SO_4)_3.7H_2O$ and $FeSO_4.7H_2O$, was made with the same concentration ratio, and its concentration was first analyzed using Inductively Coupled Plasma (ICP) as initial metal content data. A total of 20 mg of biosorbent composite was added to 20 mL of synthetic liquid waste, then stirred at a speed of 200 rpm for 2 hours. The solution was filtered, and the filtrate obtained was analyzed by ICP. The analysis results of metal content using ICP before and after the adsorption process will be compared and the efficiency percentage will be calculated. For the application in real samples, the same treatment was carried out but using samples a real sample from industrial liquid waste in Cilegon. While the solid biosorbent that has been used was dried and characterized using EDX to observe the percentage of metals adsorbed onto the biosorbent. The morphology of the biosorbent composite was characterized using Scanning Electron Microscope (SEM). The percentage efficiency of adsorption is obtained by:

$$R = \frac{C0 - C1}{C1} \; x \; 100\%$$

Were C0 and C1 is concentration of solution before and after adsorption, respectively.

3. RESULTS AND DISCUSSION

In this research, the author used organic vegetable waste as a source of humic acid and peanut shells which are converted into active carbon to carry out a waste valorization procedure. Organic waste was previously composted for 1 month, before being extracted into humic acid. These two materials are then

composed into a biosorbent which aims to adsorb metal ions. Performance tests were conducted on laboratory samples consisting of a mixture of Pb, Fe, and Al metals prior to testing on actual samples in the form of industrial waste testing with instruments such as FTIR, XRD, SEM-EDX and ICP has been carried out to support data interpretation.

3.1. Peanut Shell Activated Carbon Preparation

The process of making activated carbon goes through two stages, namely carbonization and activation. Since carbonization produces carbon has a low absorption capacity, activation is necessary to expand the carbon pores surface area. For the lignocellulosic materials, activation process used H_3PO_4 is better compared to alkaline activators because acid activators can form functional groups that contain oxygen and provide hydrophilic properties to activated carbon [14, 15]. After the activation process, the carbon is then neutralized and dried.

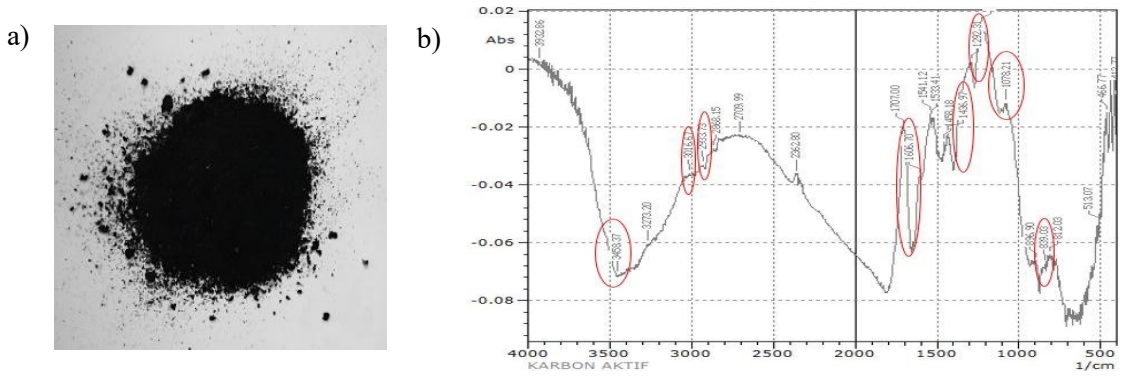

Figure 1. (a) Activated Carbon from Peanut Shell (b) FTIR Characterization of Activated Carbon

The identification of active carbon functional groups in peanuts was analyzed using FTIR. With this instrument, the chemical structure of a activated carbon can be analyzed by examining its molecular bonds and composition.

The FTIR spectrum of activated carbon has an absorption band at a wavelength of 3458.37 cm^{-1} which is the OH functional group, strengthened by the presence of C−O vibrations from secondary OH at 1078.21 cm^{-1}. The absorption at 2933.73 cm^{-1} shows the presence of aliphatic C−H stretching, reinforced by the absorption at 1436.97 cm^{-1} which is an acetylene vibration. The aromatic C−H strain is found at wave numbers 839.03 cm^{-1} and 3016.67 cm^{-1}. The C=O group is a typical group found in active carbon, shown at wave number 1606.70 cm^{-1}. Carbon bound to organic phosphate because of H_3PO_4 activation is shown at a wave number of 1292.31 cm^{-1} [16,17]. This research result is confirmed by research from Mohtashami et al. who conducted carbon activation of sugarcane bagasse with H_3PO_4. This research shows the peak spectra of FTIR in nearly the same region, In Mohtashami's et al. (2021) research, the broad intense peak at 3400 cm^{-1} represents the stretching vibration of O−H bonds in phenolic functional groups and carboxylates, meanwhile OH− bond in our research appeared in 3458.37 cm^{-1}. The stretching vibration of C−H bonds cause vibrations around 2900 cm^{-1} and 1450 cm^{-1}. And we obtained the bond of aliphatic C−H at 2933.73 cm^{-1}.

The C=O bond is present in the structures of ketones, aldehydes, lactones, or carboxyl groups, resulting in a small peak around 1700 cm^{-1}. In our research, the C=O appears in the region of 1606.70 cm^{-1}. Thus, the FTIR results of the activated carbon we produced show the appropriate characteristic peaks [30]. Activated carbon resulting from roasting peanut shells and FTIR characterization is shown in Figure 1.

The quality of activated carbon as an adsorbent was carried out on two parameters, namely water content and iodine absorption

capacity, which referred to SNI 06-3730-1995, can be seen in Table 1.

Table 1. Result of Activated Carbon Quality

Parameter	Result	SNI 06-3760-1995 Specification
Water content (%)	5	Maks. 15
Iodine absorption capacity (mg/g)	24.890	Min. 750

3.2. Result of Compost Production

Samples were made using composted organic waste and horse dung through a humification method. This compost will be used as a source of humic acid. The characteristics of the compost produced meet SNI 19-7030-2004 with test parameters for texture, odor, and color which can be seen in Table 2.

Table 2. Characterization of Compost

Parameter	Result	SNI 19-7030-2004 Specification
Texture	Not Fibrous	Not Fibrous
Odor	Smell like earth	Smell like earth
Color	Blackish Brown	Black

Based on these three parameters, it can be concluded that the results of the humification of organic waste and horse manure have successfully transformed into compost. This compost will then be extracted into humic acid.

3.3. Humic Acid Extraction

The extraction of humic acid is carried out using the compost previously prepared. The extraction is performed using NaOH solution to separate humate and vulvate contained in the compost. Purification process of Crude humic with a HCl and HF solution. The purification results then washed with distilled water and dried. The extract of humic acid that had been dried was characterized using FTIR and XRD.

This characterization result is confirmed by other research to compare the obtained results. The broad and dull absorption peak occurring at 3450 cm^{-1} can be associated with the stretching vibration of −OH in −COOH, phenol, and alcohol. While our FTIR spectrum of humic acid has an OH absorption band at a wavelength of 3525.88 cm^{-1}, strengthened by the presence of OH bending and stretching vibrations from the carboxylate group at a wavelength of 1226 cm^{-1}. There is an aromatic component structure for the C=O stretching vibration of the −COOH group at a wavelength of 1705.07 cm^{-1}. The strong vibration peak approaching 1640 cm^{-1} is associated with the stretching vibration of C=C in the benzene ring, then our resulted C−C from the aromatic ring at 1514.12 cm^{-1} and aliphatic C-H at a wavelength of 2937.59 cm^{-1}.

Although not identical, the range we obtained is similar. Therefore, to further confirm, we used XRD. XRD used to confirm the structure of humic acid based on their diffraction patterns [18]. XRD analysis is carried out on solid substances. These results were also confirmed through X-ray diffractograms compared with JCPDS. The two theta peaks indicate results that indicate humic acid peaks at 2θ = 10, 30, and 40 degrees [19,20]. From the XRD peaks, it appears that the purity of the humic acid is still not sufficiently high. However, with the presence of several matching characteristic peaks, we conclude that the synthesized humic acid has been formed. The results of the humic acid analysis can be seen in Figure 2.

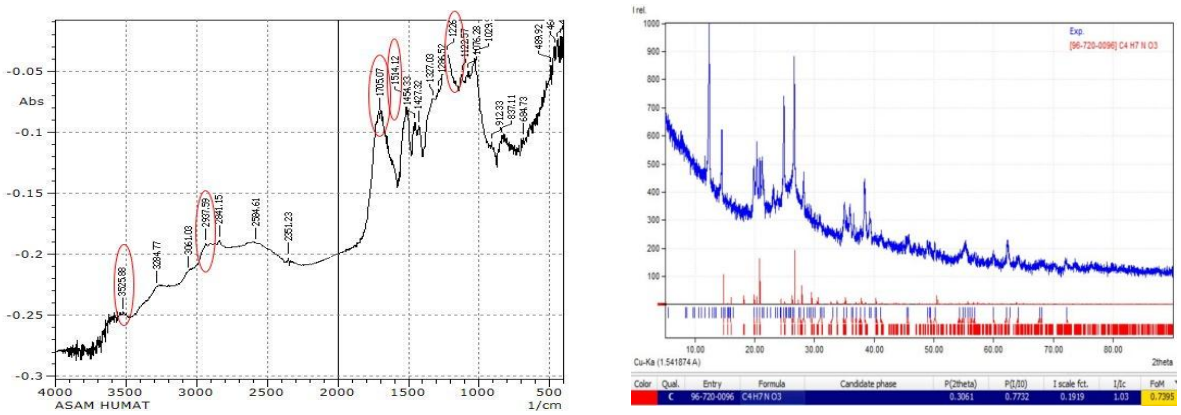

Figure 2. The Result of Humic Acid Analysis (a) FTIR Characterization of Humic Acid (b) XRD characterization of Asam Humic Acid

While natural humification is a geochemically protracted process requiring decades to millennia, recent advances in biotechnology and catalytic chemistry have demonstrated that the formation of humic-like substances (HLS) can be substantially accelerated under controlled conditions. Several studies have demonstrated that short-term composting (30–60 days) can yield materials rich in humic-like substances that exhibit similar functional groups and characteristics to naturally formed humic acids. Recent studies demonstrate that microbial-mediated biotransformation can significantly accelerate humic acid (HA) formation under controlled conditions. For instance, Zhang et al. (2022) showed that co-inoculation of *Basillus subtilis* and *Aspergilus fumigatus* during composting enhanced HA production by 53% within 35 days, with ^{13}C-NMR confirming a 38% increase in aromaticity and FTIR revealing characteristic HA functional groups (1725 cm^{-1} carboxyl, 3400 cm^{-1} phenolic −OH) [31].

This aligns with earlier work by Jurado et al. (2015), where *Trichoderma reesei* and Bacillus subtilis increased HA aromaticity by 42% in 40 days, confirming microbial consortia can replicate natural humification processes in weeks rather than years.

Both studies employed rigorous validation (IHSS protocols, enzymatic activity assays, and spectral analysis) to prove the structural equivalence of microbially synthesized HA to natural standards, offering scalable strategies for sustainable HA production [32]. In this study, the microbial mediation process used EM4 bacteria. The composting process lasted for 30 days, as described based on the research method by Maimunawaroh [33].

3.4. Biosorbent Performance Results

Compositing process of activated carbon and humic by stirring for 12 hours without the use of a cross-linking agent, allowing electrostatic forces to be the only means of interaction between the two. Activated carbon provides adsorption sites that are wide enough to allow the metal to diffuse into the pores of the biosorbent composite, while humic acid has −COOH, −OH phenolic, and −OH alcoholic groups that act as electron pair donors. The adsorption mechanism occurs when the −COOH group experiences H^+ deprotonation under alkaline conditions adjusted to the Tris buffer pH 8.5 due to the presence of OH^- ions [21,22, 23]. That's when ion exchange occurs which causes the carboxylate group to have a negative charge (COO−) and tend to bind with metal ions [24,25]. The interaction process of metal cations with the active groups of the bioadsorbent composite can be seen in Figure 3.

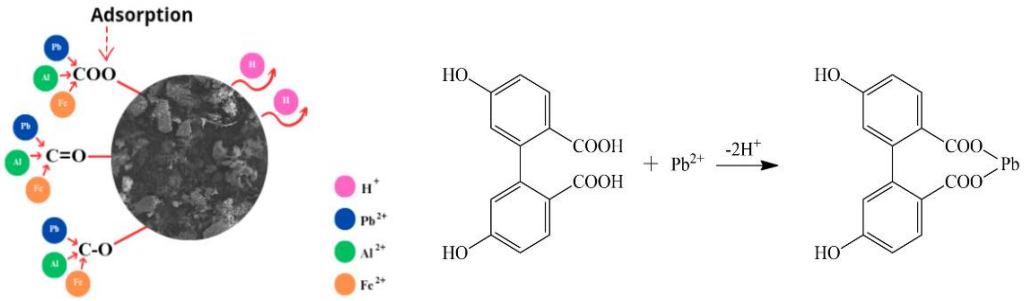

Figure 3. Mechanism of Ion Metal Adsorption

The ability of biosorbents to adsorb metals was measured using ICP. Adsorption efficiency and capacity were tested on the analyte content parameters Pb, Al, and Fe using artificial waste with concentrations containing 0.1 and 1 ppm for each metal and on real samples from Ciwandan, one of subdistrict in Cilegon City, waters in batches. The ICP instrument was chosen due to its accuracy and sensitivity in detecting the presence of metals. Furthermore, in this study, the three metals are mixed into one during the adsorption process, making the use of ICP expedient for the analysis process in terms of time. The determination of adsorbent efficiency states the percent of metal content that can be adsorbed, while adsorption capacity states the ability of an adsorbent to adsorbate. The efficiency value calculation, as mentioned in the method, involves analyzing the effectiveness of the adsorption process in removing pollutants from the solution. It is known that the percentage efficiency of 2 hours of contact time ranges from 19.5019-96.4978%. The best adsorption results were found on Pb metal with a concentration of 10 ppm, namely 96.4978%, which means 96.4978% of the total adsorbed mass was adsorbed or 0.9203 mg/g. The complete results of metal adsorption efficiency can be seen in Table 3.

Anggriani *et al.* reported that the adsorption efficiency of coconut shell-activated carbon on Pb metal was 85.6% [26], while the adsorption efficiency of humic acid on Pb metal of 54.06% [27]. The results of activated carbon adsorption on Fe metal showed an efficiency value of 44% [28], while the efficiency of adsorption of Fe metal by humic acid was 34.78%. It can be concluded that the results of the adsorption efficiency of Pb and Fe metals in this research are relatively greater compared to several previous studies. In this study, the three metals are mixed into one solution during the adsorption process.

Table 3. Results of Metal Adsorption Efficiency

Sample Concentration (ppm)	Adsorption Efficiency		
	Pb	Fe	Al
1	74,210	58,696	41,351
10	96,498	45,216	19,502

The adsorption capacity of Fe is relatively low, possibly due to the stronger attraction of Pb, leading Pb to occupy the biosorbent pore sites first, while Fe fills the remaining available pores. As for Al metal, the efficiency value is relatively small compared to Pb and Fe metals. This is because the Al^{3+} ions react first with phosphate ions which come from the activated carbon activation process to form $AlPO_4$ resulting in the number of Al^{3+} ions in the solution being reduced so that the adsorption efficiency decreases [29,30]. In this research, real sample testing was carried out in Ciwandan waters, resulting in Pb, Al, and Fe adsorption efficiencies of 66.50%, 36.16%, and 50.96% respectively. The efficiency results of testing on real samples are relatively lower compared to synthetic (laboratory) samples. This is because there are more matrices present in real samples. Since in this

study, the real samples were not destructed beforehand but directly adsorbed with the biosorbent.

3.5. Morphology and Composition of Biosorbent

Adsorption ability can be influenced by the average pore diameter of the adsorbent. The larger the average pore diameter of the adsorbent, the better the adsorption efficiency. SEM is used to analyze the surface morphology of a material; in this case, the analysis reveals the pores of the bioadsorbent composite. The pore diameter measured by ImageJ software. Based on the calculation of the average distribution of the adsorbent pore diameter, the result was 4,344 µm.

Enough pore diameter exists for effective adsorbate adsorption. After the adsorption process, the pore cavity of the adsorbent appears to be more filled with adsorbate. This is shown by the surface morphology via SEM images at 500x dan 1000x magnification. The average distribution of the adsorbent pore diameter upon adsorption decreased by 1,216 µm, according to the measurement data. The surface morphology before and after the adsorption process can be seen in Figure 4.

Image 4a shows the morphology before the adsorption process. From the indicated arrows, the pores of the biosorbent are still wide. It is at these sites that metals will be adsorbed. In Figure 4b, after the adsorption process, the pore image appears fuller. This is because the pores are now filled with metals that have been adsorbed at those sites. To ensure that the pores have indeed been filled with metals after the adsorption process, characterization with EDX is conducted.

EDX is utilized to determine the elemental composition of biosorbent composites after they have been used for metal adsorption. Based on measurements with EDX, the elemental composition after the adsorption process can be identified by the appearance of Pb, Al, and Fe spectrum peaks respectively with atomic abundance percentages of 0.39%, 0.47%, and 0.85%. The EDX graph after trapping can be seen in Figure 5.

With the detection of Pb, Al, and Fe metals used EDX, which are the pollutants used in this study, it proves that the material filling the pores of the biosorbent in the SEM image is indeed waste metal. Thus, the biosorbent we have created can effectively absorb these metals.

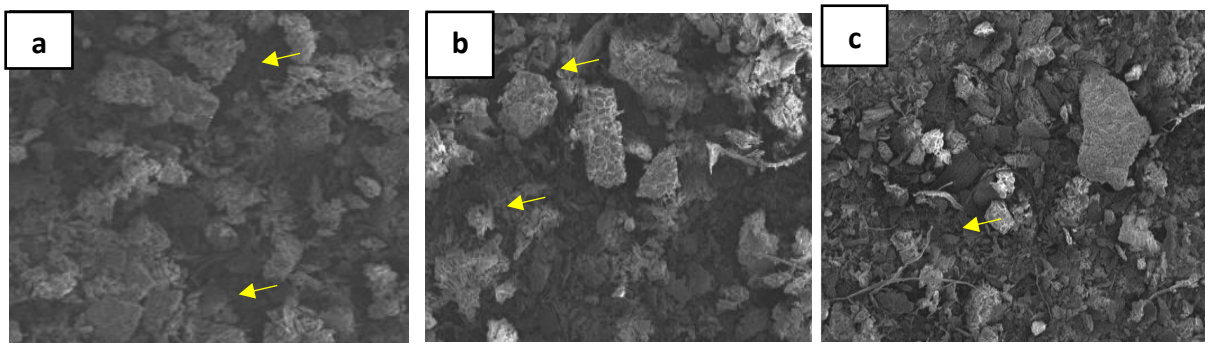

Figure 4. Morphology of Bioadsorbent Composite (a) Before Heavy Metal Adsorption 500x (b) After Heavy Metal Adsorption 500x (c) After Heavy Metal Adsorption 1000x

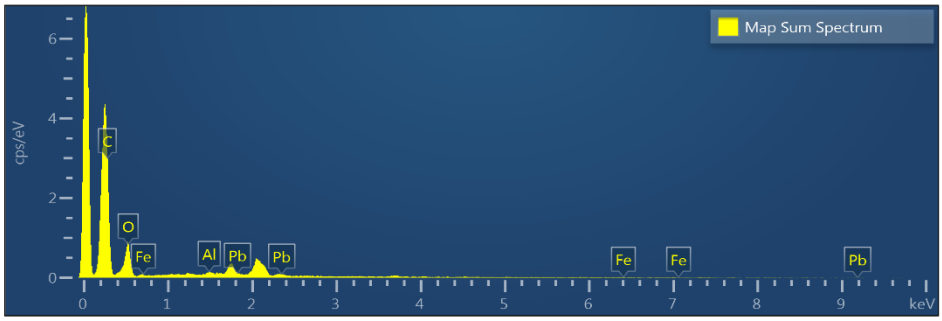

Figure 5. EDX Result After Adsorption

This study is an initial exploration into combining the functions of activated carbon and humic acid as absorbents. The results obtained are quite satisfactory, with a good adsorption performance. However, further research on the formula or ratio comparison of activated carbon and humic acid used would provide more characteristic information. This aims to determine the composition that provides the best efficiency in adsorbing various types of metals.

4. CONCLUSIONS

A biosorbent composite based on peanut shells and organic waste has been synthesized. The synthesized biosorbent composite has a macro pore size that can adsorb Pb^{2+} and Fe^{2+} metals efficiently, with adsorption percentages reaching 96.49% and 58.69%, respectively. Meanwhile, Al^{3+} adsorption has a smaller efficiency value because Al^{3+} ions react first with phosphate ions to form $AlPO_4$. Overall, this research can be applied to reduce industrial waste samples, Since the adsorption efficiency percentage is already more than 50%, with the best result reaching over 90%. To achieve a better efficiency value, more research is necessary to determine the exact amounts of each substance (humic acid and active carbon) and the adsorption experiments were conducted separately for each metal. This biosorbent is very prospective to be developed to overcome environmental problems.

ACKNOWLEDGMENT

Thanks are conveyed to the BELMAWA Directorate of the Ministry of Education, Culture, Research, and Technology for funding research on the student creativity program (PKM) in the field of research and Sekolah Tinggi Analis Kimia Cilegon for funding and providing laboratory facilities

LIST OF REFERENCES

Republik Indonesia, “Keputusan Menteri Lingkungan Hidup dan Kehutanan Republik Indonesia tentang Hasil Penilaian Peringkat Kinerja Perusahaan dalam Pengelolaan Lingkungan Hidup Tahun 2021-2022."Jakarta, 2023. [Online]. Available: https//proper.menlhk.go.id/proper/berita/detail/366

J. J. Frank, A. G. Poulakos, R. Tornero-Velez, and J. Xue, “Systematic review and meta-analyses of lead (Pb) concentrations in environmental media (soil, dust, water, food, and air) reported in the United States from 1996 to 2016,” *Sci. Total Environ.*, vol. 694, p. 133489, 2019, doi: 10.1016/j.scitotenv.2019.07.295.

R. Chakraborty, A. Asthana, A. K. Singh, B. Jain, and A. B. H. Susan, “Adsorption of heavy metal ions by various low-cost adsorbents: a review,” *Int. J. Environ. Anal. Chem.*, vol. 102, no. 2, pp. 342–379, 2022, doi: 10.1080/03067319.2020.1722811.

Indonesia,“Badan Pusat Statistik Kota Cilegon, Kota Cilegon dalam Angka; 2021.” BPS Kota Cilegon, 2021. [Online]. Available: https://cilegonkota.bps.go.id/publication/2021/02/26/62579c317955d0838eef1313/kota-cilegon-dalam-angka-2021.html

H. Xu *et al.*, “Cd(II) and Pb(II) absorbed on humic acid-iron-pillared bentonite: Kinetics, thermodynamics and mechanism of adsorption,” *Colloids Surfaces A Physicochem. Eng. Asp.*, vol. 612, no. Ii, 2021, doi: 10.1016/j.colsurfa.2020.126005.

P. Kulal and V. Badalamoole, “Hybrid nanocomposite of kappa-carrageenan and magnetite as adsorbent material for water purification,” *Int. J. Biol. Macromol.*, vol. 165, pp. 542–553, 2020, doi: 10.1016/j.ijbiomac.2020.09.202.

M. I. Shafi *et al.*, “Application of single superphosphate with humic acid

improves the growth, yield and phosphorus uptake of wheat (Triticum aestivum L.) in calcareous soil," *Agronomy*, vol. 10, no. 9, pp. 1–15, 2020, doi: 10.3390/agronomy10091224.

O. Bezuglova and A. Klimenko, "Application of Humic Substances in Agricultural Industry," *Agronomy*, vol. 12, no. 3, 2022, doi: 10.3390/agronomy12030584.

J. Tiwari, A. L. Ramanathan, K. Bauddh, and J. Korstad, "Humic substances: Structure, function and benefits for agroecosystems—a review," *Pedosphere*, vol. 33, no. 2, pp. 237–249, 2023, doi: https://doi.org/10.1016/j.pedsph.2022.07.008

H. Li *et al.*, "Efficient removal of water pollutants by hierarchical porous zeolite-activated carbon prepared from coal gangue and bamboo," *J. Clean. Prod.*, vol. 325, p. 129322, 2021, doi: https://doi.org/10.1016/j.jclepro.2021.129322.

H. Liu, C. Cheng, and H. Wu, "Sustainable utilization of wetland biomass for activated carbon production: A review on recent advances in modification and activation methods," *Sci. Total Environ.*, vol. 790, p. 148214, 2021, doi: 10.1016/j.scitotenv.2021.148214.

J. Shahrivar and M. Gharabaghi, "Separation of $AuCN^{2-}$ by activated carbon and functionalized graphene/activated carbon composite," *Adv. Powder Technol.*, vol. 31, no. 12, pp. 4648–4656, 2020, doi: 10.1016/j.apt.2020.10.005.

Z. Li *et al.*, "Adsorption of congo red and methylene blue dyes on an ashitaba waste and a walnut shell-based activated carbon from aqueous solutions: Experiments, characterization and physical interpretations," *Chem. Eng. J.*, vol. 388, no. January, p. 124263, 2020, doi: 10.1016/j.cej.2020.124263.

Y. A. B. Neolaka *et al.*, "Indonesian Kesambi wood (Schleichera oleosa) activated with pyrolysis and H_2SO_4 combination methods to produce mesoporous activated carbon for Pb(II) adsorption from aqueous solution," *Environ. Technol. Innov.*, vol. 24, p. 101997, 2021, doi: 10.1016/j.eti.2021.101997.

S. M. Kharrazi, N. Mirghaffari, M. M. Dastgerdi, and M. Soleimani, "A novel post-modification of powdered activated carbon prepared from lignocellulosic waste through thermal tension treatment to enhance the porosity and heavy metals adsorption," *Powder Technol.*, vol. 366, pp. 358–368, 2020, doi: 10.1016/j.powtec.2020.01.065.

G. K. P. Lopes *et al.*, "Steam-activated carbon from malt bagasse: Optimization of preparation conditions and adsorption studies of sunset yellow food dye," *Arab. J. Chem.*, vol. 14, no. 3, 2021, doi: 10.1016/j.arabjc.2021.103001.

M. Lanno, M. Klavins, O. Purmalis, M. Shanskiy, A. Kisand, and M. Kriipsalu, "Properties of Humic Substances in Composts Comprised of Different Organic Source Material," *Agric.*, vol. 12, no. 11, pp. 1–14, 2022, doi: 10.3390/agriculture12111797.

D. Zingaretti, M. A. Lominchar, I. Verginelli, A. Santos, and R. Baciocchi, "Humic acids extracted from compost as amendments for Fenton treatment of diesel-contaminated soil," *Environ. Sci. Pollut. Res.*, vol. 27, no. 18, pp. 22225–22234, 2020, doi: 10.1007/s11356-020-

08221-5.

R. Basuki, B. Rusdiarso, S. J. Santosa, and D. Siswanta, "Magnetite-Functionalized Horse Dung Humic Acid (HDHA) for the Uptake of Toxic Lead(II) from Artificial Wastewater," *Adsorpt. Sci. Technol.*, vol. 2021, 2021, doi: 10.1155/2021/5523513.

N. A. Bakar *et al.*, "An insight review of lignocellulosic materials as activated carbon precursor for textile wastewater treatment," *Environ. Technol. Innov.*, vol. 22, p. 101445, 2021, doi: 10.1016/j.eti.2021.101445.

P. Zhao, Z. Huang, Q. Ma, B. Zhang, and P. Wang, "Artificial humic acid synthesized from food wastes: An efficient and recyclable adsorbent of Pb (II) and Cd (II) from aqueous solution," *Environ. Technol. Innov.*, vol. 27, p. 102399, 2022, doi: 10.1016/j.eti.2022.102399.

X. Chen, X. Yang, Y. Xiang, L. Xu, and G. Liu, "Humic Acid Derived Resin: An Efficient Adsorbent for Au(III) Uptake from Aqueous Acidic Solution," *J. Chem. Eng. Data*, vol. 65, no. 4, pp. 1824–1832, 2020, doi: 10.1021/acs.jced.9b01085.

T. Alomar, H. Qiblawey, F. Almomani, R. I. Al-Raoush, D. S. Han, and N. M. Ahmad, "Recent advances on humic acid removal from wastewater using adsorption process," *J. Water Process Eng.*, vol. 53, no. January, p. 103679, 2023, doi: 10.1016/j.jwpe.2023.103679.

S. Mandal, J. Calderon, S. B. Marpu, M. A. Omary, and S. Q. Shi, "Mesoporous activated carbon as a green adsorbent for the removal of heavy metals and Congo red: Characterization, adsorption kinetics, and isotherm studies," *J. Contam. Hydrol.*, vol. 243, no. March, p. 103869, 2021, doi: 10.1016/j.jconhyd.2021.103869.

U. Meila Anggriani *et al.*, "Kinetika adsorpsi karbon aktif dalam penurunan konsentrasi logam tembaga (Cu) dan timbal (Pb)," *J. Kinet.*, vol. 12, no. 02, pp. 29–37, 2021, [Online]. Available: https://jurnal.polsri.ac.id/index.php/kimia/index

D. Umaningrum, D. Rasy Mujiyanti, R. Nurmasari, J. A. Yani Km, and B. Kalimantan Selatan, "Adsorpsi Pb (II) Oleh Asam Humat Terimobilisasi Pada Hibrida Merkapto Silika Dari Abu Sekam Padi," *J. Sains dan Terap. Kim.*, vol. 8, no. 1, pp. 20–26, 2016, [Online]. Available: https://ppjp.ulm.ac.id/journal/index.php/jstk/article/view/2130

R. Siskayanti, "Efektifitas Arang Aktif dari Tempurung Kelapa dalam Mengadsorpsi Logam Fe pada Pelumas Motor Bekas Pakai," *J. Redoks*, vol. 5, no. 2, p. 108, 2020, doi: 10.31851/redoks.v5i2.4990.

R. D. Rios, P. J. Bueno, J. C. Terra, and F. C. Moura, "Influence of the surface modification of granular-activated carbon synthesized from macauba on heavy metal sorption," *Environ. Sci. Pollut. Res.*, vol. 30, no. 11, pp. 31881–31894, 2023.

L. S. Miranda, B. Wijesiri, G. A. Ayoko, P. Egodawatta, and A. Goonetilleke, "Water-sediment interactions and mobility of heavy metals in aquatic environments," *Water Res.*, vol. 202, no. February, p. 117386, 2021, doi: 10.1016/j.watres.2021.117386.

S. A. Mohtashami, N. Asasian Kolur, T. Kaghazchi, R. Asadi-Kesheh, and M.

Soleimani, “Optimization of sugarcane bagasse activation to achieve adsorbent with high affinity towards phenol,” *Turkish J. Chem.*, vol. 42, no. 6, pp. 1720–1735, 2018, doi: 10.3906/kim-1806-71.

D. Wu, W. Gao, Y Zhao, Z.Wei, C . Song, F. Qu, F. Wang. "Elaborating the microbial mechanism of humic substance formation during lignocellulosic biomass composting by inoculation with different functional microbes," *Ind. Crops Prod.*, vol. 187, p. 115481, Nov. 2022, doi: 10.1016/j.indcrop.2022.115481.

M. M. Jurado, F.S Estrella, M.J Lopez, M.C Vargas-Gracia. "Enhanced turnover of organic matter fractions by microbial stimulation during lignocellulosic waste composting," Bioresour. Technol., vol. 186, pp. 179-186, Jun. 2015, doi: 10.1016/j.biortech.2014.11.089.

Maimunawaro, S. K. Rahman, and C. Irawan, "Pemanfaatan asam humat dari sampah organik sebagai adsorben pada limbah cair sintesis timbal (Pb)," *J. Teknol. Kim. Indones.*, vol. 19, no. 1, pp. 26-32, Apr. 2020, doi: 10.5614/jtki.2020.19.1.5.

JURNAL ILMIAH BERKALA SAINS DAN TERAPAN KIMIA

Jurnal Ilmiah Berkala: Sains dan Terapan Kimia
Vol. 19 No. 2, Juli 2025

Larvacidal And *Oviposition Deterrent* Activity of Dragon Scale Fern (*Pyrrosia piloselloides* (L.) M. G. Price) Extract Against *Culex sp.*

Uji Aktivitas Larvasida dan *Oviposition Deterrent* Ekstrak Paku Sisik Naga (*Pyrrosia piloselloides* (L.) M. G. Price) terhadap Nyamuk *Culex sp.*

Khodijah Amini Tanjung[1], Halimatussakdiah Halimatussakdiah [1*], and Muslimah Muslimah

[1]Chemistry, Faculty of Science and Technology, Samudra University, Jl. Prof. Dr. Syarief Thayeb, Langsa, 24416, Indonesia.

*Email: halimatussakdiah@unsam.ac.id

ABSTRACT

Dragon scale fern (Pyrrosia piloselloides (L.) M. G. Price) is one of the plants that grows and spreads wild throughout the tropics and this plant is an epiphyte (a plant that attaches to the stems of other plants), but is not a parasite because this plant can make its own food. This study aims to test the larvicidal and oviposition deterrent activities of the methanol extract of dragon scale fern. Dry leaves of P. piloselloides (L.) M. G. Price were macerated with methanol to produce 30.5 g of methanol extract. Methanol extract contained secondary metabolites compounds of steroid, saponin, flavonoid, and tannin. The methanol extract was tested for larvicidal and oviposition deterrent activities against Culex sp. mosquitoes with concentrations of 31.25; 62.50; 125; 250; 500; 1000; and 2000 ppm. The results showed strong larvicidal activity (toxic) with an LC_{50} value of 143 ppm, and oviposition deterrent activity produces % ER of 72% at a concentration of 2000 ppm. The results of the study showed that methanol extract of dragon scale fern can be used as a natural larvicidal and oviposition deterrent, this activity is contributed by the presence of secondary metabolite compounds, especially flavonoids, saponins, tannins, and steroids.

Keywords: Dragon scale fern (*P. piloselloides* (L.) M. G. Price), mosquito larvae, oviposition deterrent.

ABSTRAK

Paku sisik naga (Pyrrosia piloselloides (L.) M. G. Price) adalah salah satu tumbuhan yang tumbuh dan tersebar secara liar di seluruh daerah tropis dan tumbuhan ini merupakan tumbuhan epifit (tumbuhan yang menempel pada batang tumbuhan lain), tapi bukan parasit karena tumbuhan ini dapat membuat makannya sendiri. Penelitian ini bertujuan untuk menguji aktivitas larvasida dan oviposition deterrent dari ekstrak metanol paku sisik naga. Daun kering P. piloselloides (L.) M. G. Price dimaserasi dengan metanol menghasilkan ekstrak metanol sebanyak 30,5 g. Ekstrak metanol mengandung senyawa metabolit sekunder golongan steroid, saponin, flavonoid, dan tanin. Ekstrak metanol diuji aktivitas larvasida dan oviposition deterrent terhadap nyamuk Culex sp. dengan konsentrasi 31,25; 62,50; 125; 250; 500; 1000; dan 2000 ppm. Hasil pengujian diperoleh aktivitas larvasida yang kuat (toksik) dengan nilai LC_{50} 143 ppm, dan aktivitas oviposition deterrent menghasilkan % ER sebesar 72% pada konsentrasi 2000 ppm. Hasil penelitian menunjukkan bahwa ekstrak metanol paku sisik naga dapat dijadikan sebagai larvasida dan oviposition deterrent alami, aktivitas tersebut dikontribusi oleh adanya kandungan senyawa metabolit sekunder, khususnya golongan flavonoid, saponin, tanin, dan steroid.

Keywords: Paku sisik naga (*P. piloselloides* (L.) M. G. Price), larvasida nyamuk, *oviposition deterrent*

Received: 14 January 2025 ; **Accepted**: 26 July 2025: **Available online**: 30 July 2025

1. INTRODUCTION

Indonesia is one of the world's richest countries in terms of biodiversity. Sources of biodiversity in Indonesia play an important role in all communities. People, especially in rural areas, tend to use plants as traditional medicines to treat diseases. Data show that there are about 30,000 species of flora in Indonesia's tropical forests, and about 9,600 plant species are known to have medicinal benefits (Nola at al, 2021).

One type of plant that has been used as a traditional medicine is the dragon scale fern (*Pyrrosia piloselloides* (L.) M.G. *Prece*). This epiphytic plant is often found attached to the stems of plants. Although this plant appears to be of no value, dragon scale fern has functions and properties as a medicinal plant, both fresh and dried. This plant is used to treat various ailments such as gingivitis, mouth ulcers, rheumatism, tuberculosis (TB) glands (scrofula) and breast cancer (Kamal, Prayitno and Hamdi, 2021). Dragon scale fern produces various bioactive compounds that can be used as antibacterial, antipyretic, anticancer and antioxidant (Asiandu, Widjajanti and Nurnawati, 2019). Dragon scale fern belongs to the *Polypodiaceae* family. Several studies have reported that plants belonging to the *Polypodiaceae* family have larvicidal activity, such as the *Drynaria quercifolia* plant used in synthesizing nanoparticles have larvicidal activity against *Culex quinquefasciatus* mosquitoes with an LC50 (Lethal Concentration 50) value of 130.725 ppm (Kalaimurgan et al., 2023). Santos et al., 2023 reported that the *Microgramma vacciniifolia* plant is a family of *Polypodiaceae* and stated that the extract from the plant showed larvicidal potential against *Alphitobius diaperinus* larvae. In addition, other plants of the *Polypodiaceae* family have larvicidal and pupicidal effects, namely ethanol extract of the roots and rhizomes of *Dryopteris filix-mas* against the third instar larvae of *Corcyra cephalonica*, where *D. filix-mas* extract 0.20% (v/w) can cause 100% larval death (Shukla, 2011). According to plant taxonomy, the same family has similar chemical content, so it is thought to have the same biological activity (Sukaeningsih, Sukandar and Qowiyyah, 2021).

Larvicide is a method of mosquito larvicide control that is often used by the community because it has several advantages, namely rapid results, ease of use, effectiveness, availability and low cost (Yuliana et al., 2021). Methods to control the spread of mosquito larvae can be biological, chemical and physical. Synthetic larvicides are usually used for larval control because they are very effective, relatively cheap, easy and convenient to use. One of the synthetic larvicides commonly used in the Community is 1% Abate (*Temephos*). However, the continuous use of abate has very dangerous effects, one of which is the contamination of water, especially drinking water. The many negative effects of synthetic larvicides have limited their use. Therefore, the development of natural larvicides is needed to reduce the negative effects of synthetic larvicides (Ekayani et al., 2021). The compounds that have potential as larvicides are flavonoids, saponins, tannins, alkaloids and steroids (Tutik and Marcellia, 2021; Melita, Elsyana and Ulfa, 2022).

In addition to larvicides, oviposition deterrents are also used to control mosquitoes. Oviposition deterrent is a method of inhibiting egg deposition by using chemical compounds to prevent egg deposition. Inhibition of egg deposition provides valuable information that can be manipulated to manage the population.

Mosquitoes are among the animals that become vectors of various diseases. Culex sp. mosquitoes are known as a type of mosquito vector known as the house mosquito. Some types of diseases that can be transmitted by Culex mosquitoes are Japanese Encephalitis (JE) or called an inflammatory brain disease that affects animals and humans, Louis Encephalitis, a disease that attacks the central

nervous system in humans and lymphatic filariasis or called elephantiasis (Hestiningsih et al., 2019).

Based on the above literature, there is a need to develop a natural mosquito control method against Culex sp. Today, no research has been conducted on the use of dragon scale fern for larvicidal and oviposition deterrent testing. However, there are references to plants in the *Polypodiaceae* family having anti-mosquito activity. Therefore, dragon scale fern also has the potential to act as larvicides and oviposition deterrents to control mosquitoes such as Culex sp.

2. MATERIALS AND METHODS

2.1. Materials

The materials used in this study are aquadest, sugar solution, 98% methanol (CH_3OH), ethyl acetate ($C_4H_8O_2$), n-hexane (C_6H_{14}), dimethylsulfoxide (DMSO), ammonia (NH_3), chloroform ($CHCl_3$), sulfuric acid (H_2SO_4), ferric chloride ($FeCl_3$), Mayer reagent, Dragendorff reagent, Wagner reagent, Lieberman-Burchard reagent (CH_3COOH and H_2SO_4), hydrochloric acid (HCl), ethanol (C_2H_5OH), 10% NaOH solution, mice and Abate solution. The tools used in this research are gloves, masks, glass beakers, Erlenmeyer flasks, filter paper, spatulas, glass jars, beakers, test tubes, tube racks, dropping pipettes, analytical balances, rotary evaporators, funnels, plastic pipettes, aluminium foil, measuring cups, plastic wrap, knives, plastic beakers, watch glasses, gauze, plastic tubs, label paper, mosquito cages, drip plates and canister.

2.2. Sample Preparation and Extraction

A total of 500 g of dried and cut dragon scale fern (*P. piloselloides* (L.) M. G. Price) underwent extraction through a multistage maceration process utilizing n-hexane, ethyl acetate, and methanol as solvents. The maceration was conducted over three cycles of 72 hours each and continued until the filtrate became clear (Halimatussakdiah, Amna and Wahyuningsih, 2018). The resulting extract solutions were filtered and concentrated using a rotary evaporator to obtain n-hexane, ethyl acetate, and methanol extracts. In this study, the methanol extract was used.

2.3. Phytochemical Test

Phytochemical test is one way of identifying the content of secondary metabolites in a natural material. Phytochemical tests were carried out to identify compounds of the alkaloid, terpenoid, steroid, saponin, phenolic, flavonoid and tannin groups (Vifta and Advistasari, 2018). Phytochemical test carried out on alkaloids, terpenoids, and steroids, saponins, phenolics, and tannins in the manner as reported by Halimatussakdiah, Amna and Wahyuningsih, 2018, and a flavonoid test was carried out using the method reported by Kusnadi and Devi, 2017.

2.4. Larvicidal Activity Test

The larvicidal test was carried out with 3 (three) replicates, the methanol extract was prepared in test dishes for different concentrations of 31.25; 62.50; 125; 250; 500; 1000; and 2000 ppm in aquadest. Each treatment included 10 mosquito larvae and was incubated for 48 hours. After 48 hours, live and dead mosquito larvae were counted and statistically analyzed using the Bill test method. The concentration was plotted against percent mortality to obtain a curve, and the curve obtained was used to determine the Lethal Concentration 50 (LC50) value (Halimatussakdiah, Amna and Wahyuningsih, 2018). Larvicides can be calculated as percent mortality using the formula below:

$$\%Mortality = \frac{\text{accumulated number of dead larvae}}{\text{accumulated total number}} \times 100\%$$

2.5. Oviposition Deterrent Test

Synthesis of activated carbon composite the *oviposition deterrent* experiment was conducted using *Culex sp*. mosquitoes initially housed in mosquito cages and subsequently transferred to individual cages measuring 60 cm x 50 cm x 50 cm. These cages were constructed from wood, enclosed with mosquito nets, and equipped with a cloth-covered front panel for access. Within each cage, nine plastic bowls were arranged: seven

bowls containing varying concentrations of extract solutions, one bowl serving as a positive control with temephos, and the other as a negative control. The tested concentrations were 31.25 ppm, 62.50 ppm, 125 ppm, 250 ppm, 500 ppm, 1000 ppm, and 2000 ppm, with each concentration tested in triplicate. Adult mosquitoes were provided with a 10% sugar solution as food, and occasionally, a mouse was introduced as a protein source to facilitate egg production. The experiment was conducted at room temperature over 48 hours, after which the number of eggs in each bowl was counted and documented for all concentrations (Arifin, Nasution and Halimatussakdiah, 2012; Reegan *et al.*, 2015).

The effectiveness of *oviposition deterrence* was evaluated by comparing the number of eggs in the treatment bowls to those in the negative control bowls. The *Effective Repellency* (% ER) and *Oviposition Activity Index* (OAI) were calculated using standard formulas.

$$\% \text{ ER} = \frac{NC - NT}{NC} X\ 100\%$$

$$(\text{OAI}) = \frac{\text{NT-NC}}{\text{NT +NC}}$$

Description:

% ER = Percentage of *effective repellency*
NC = Number of eggs in negative control
NT = Number of eggs in sample
OAI = *Oviposition Activity Index* (Arifin, Nasution and Halimatussakdiah, 2012).

3. RESULTS AND DISCUSSION

3.1 Extraction Results

The methanol extract was evaporated using a rotary evaporator. This resulted in 30.5 g of concentrated methanolic extract of dragon scale fern leaves.

3.2 Phytochemical Screening Results

Phytochemical screening was carried out with the aim of identifying the secondary metabolite compounds contained in the methanol extract of dragon scale fern leaves. The results of the phytochemical screening of the methanol extract showed that the methanol extract of dragon scale fern leaves contained secondary metabolites, namely steroid compounds, saponins, flavonoids and tannins, as shown in Table 1.

Table 1. Phytochemical Test Results of Dragon Scale Fern Leaf Extract (*P. piloselloides* (L.) M. G. Price.

Compound	Reagent	Result
Alkaloids	Dragendorff	-
	Mayer	-
	Wagner	-
Terpenoids	Lieberman Burchard	-
Steroids	Lieberman Burchard	+
Saponins	Aquades	+
phenolic	$FeCl_3$	-
Flavonoids	NaOH	+
Taninns	- $FeCl_3$	+

Infirmation: +: positive; -: negative

The steroid test produces a positive result when the terpenoid test yields a negative outcome. In the steroid test, a color change to green in the solution indicates the presence of steroid compounds. The positive reaction occurs due to condensation or water release, coupled with carboxylation and fusion. The process begins with the release of hydrogen atoms and their electrons, causing shifts in double bonds. This compound then undergoes resonance, acting as an electrophile during carboxylation. Carboxylation triggers

electrophilic addition, followed by the release of hydrogen atoms. Subsequently, the hydrogen atoms and their electrons are released, leading to conjugate extension of the compound. This results in the formation of a red ring, as described in (Nurjannah *et al.*, 2022). The reaction mechanism for the Lieberman-Burchard steroid test is illustrated in Figure 1.

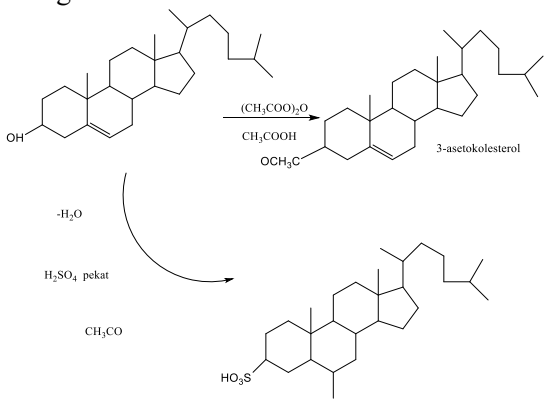

Figure 1. Mechanism of Steroid Test Reaction with Lieberman-Burchard Reagent (Putri Anggraeni, Chatri and Advinda, 2023).

Table 1 showed positive results in the saponin test in methanol extract, as evidenced by the formation of stable foam for 30 minutes, indicating the presence of glycosides with the ability to form foam in water, which are hydrolysed to glucose. The reaction that occurs during the saponin test is shown in Figure 2.

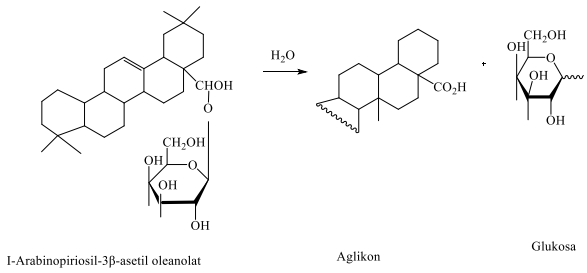

Figure 2. Reaction Mechanism for Testing the Existence of Saponin Compounds (Marlina, Suryati and Suyono, 2005)

The flavonoid test carried out showed positive results, indicated by a change in colour to yellow after testing with 10% NaOH. Crystalline compounds which are derivatives of flavonoid compounds are decomposed by bases in the addition of 10% NaOH into molecules such as acetophenone which is yellow in colour due to the breaking of bonds in the isoprene structure. The reaction mechanism of the flavonoid test with 10% NaOH is shown in Figure 3.

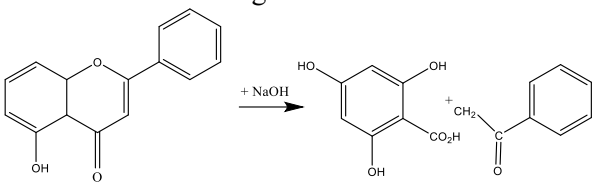

Figure 3. Flavonoid Test Reaction Mechanism with 10% NaOH (Kusnadi and Devi, 2017)

The tannin test carried out showed positive results, characterised by a brownish-green discolouration. This colour change is due to the formation of a complex compound between the Fe metal and the tannin. Complex compounds are formed due to the presence of coordination covalent bonds between metal and non-metalions (Deti Andasari, Hermanto and Wahyuningsih, 2020). The reaction mechanism that occurs in the tannin test is shown in Figure 4.

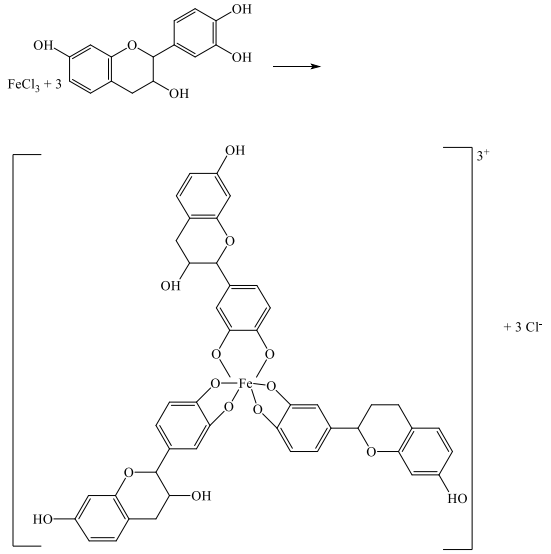

Figure 4. Reaction Mechanism of Tannin Test with $FeCl_3$ (Manongko, Sangi and Momuat, 2020)

3.3 Results of Larvicidal Activity Tests on Culex sp. Larvae

Larvicides aim to eliminate mosquito larvae using chemical compounds. Natural

larvicides offer several benefits, including their ability to break down rapidly under the influence of sunlight, air, moisture, and other environmental factors, thereby minimizing the risk of groundwater and water pollution. Additionally, natural larvicides typically exhibit low toxicity to mammals, making them safer for use around humans. When selecting extracts for use as natural larvicides, it is essential to consider their safety for humans and other organisms, as well as their potential benefits.

A larvicidal test using methanol extract was performed to evaluate the activity of secondary metabolites from the leaves of the dragon scale fern (*P. piloselloides* (L.) M.G. Price) against mosquito larvae. The test assessed larvicidal activity using the Lethal Concentration 50% (LC_{50}) parameter, which represents the concentration of a chemical substance capable of causing the death of 50% of the test organisms. The effectiveness was determined based on the number of larvae killed by the methanol extract of dragon scale fern leaves after 48 hours, as shown in Table 2.

Based on Table 2, above, there are differences in the effect of dragon scale fern leaf extract at each concentration on *Culex sp*. mosquito larvae, where the control treatment with other concentration treatments has different effects. This indicates that there is an influence of chemical compounds that are toxic in the extract so that it can cause death in *Culex sp*. mosquito larvae, so that the concentration that can kill 50% of the *Culex sp*. mosquito population (LC_{50}) can be determined. The number of larvae in Table 2 was entered and analysed in the Bill test table (Table 3) to obtain cumulative data (number of dead accumulated and number of alive accumulated), the data helped to see the overall pattern of number of deaths and survival up to each concentration. Based on these data, the % mortality can be calculated, i.e. the percentage of deaths at each concentration. The curve of % mortality vs. log concentration of the methanol extract can then be plotted in Figure 5, giving a linear regression equation to determine the LC_{50} value.

Table 2. Number of Larvae Killed by Methanol Extract of Dragon Scale Fern Leaves in Larvicidal Activity Test After 48 Hours.

Mosquito Condition	Average Number of Larvae in Methanol Extract Media at Various Concentrations (ppm)							Control (+)	Control (-)
	2000	1000	500	250	125	62.50	31.25		
Life	1	3	6	5	6	7	4	0	10
Dead	9	7	4	5	4	3	6	10	0

Information: - positive control: aquadest + abate; - negative control: aquadest

Table 3. Results of Analysis of Larvicidal Activity of Methanol Extract of Dragon Scale Fern Leaves against Culex sp. Mosquito Larvae using Bill Test Table.

Concentration Log	Death toll	Number of Lives	Accumulated Death Toll	Accumulated Life Count	Ratio	Mortality	LC_{50} (ppm)
					Totally Dead	(%)	
3.301	9	1	38	1	0.97	97.44	
3.000	7	3	29	4	0.88	87.88	
2.699	4	6	22	10	0.69	68.75	
2.398	5	5	18	15	0.55	54.55	143 ppn
2.097	4	6	13	21	0.38	38.24	
1.796	3	7	9	28	0.24	24.32	
1.495	6	4	6	32	0.16	15.79	

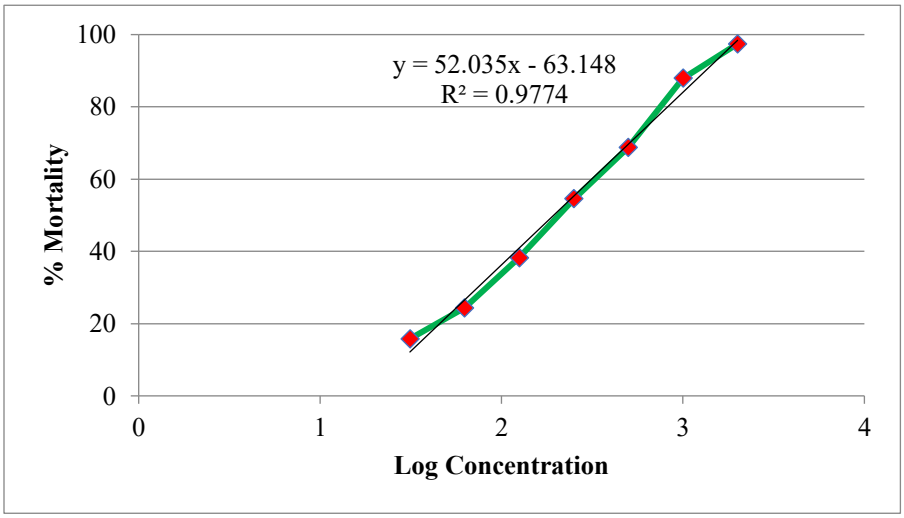

Figure 5. Larvicidal Activity Curve of Dragon Scale Fern Extract (*P. piloselloides* (L.) M. G. Price)

The LC_{50} value was calculated to determine the toxicity of the extract to the test larvae after 72 hours of observation. According to (Sumihe, Runtuwene and Rorong, 2014), the toxicity level of an extract is as follows: if $LC_{50} \leq 30$ mg/L = highly toxic, meaning that a very low concentration is required to kill 50% of the test larvae; if $LC_{50} \leq 1000$ mg/L = toxic, meaning that extracts in this range are also effective as larvicides but require higher concentrations than highly toxic extracts; and if $LC_{50} > 1000$ mg/L = non-toxic, this is considered to be non-toxic to larvae because very high concentrations are not required to achieve 50% mortality, extracts in this category are considered to be less effective as larvicides.

Based on Figure 5. The LC_{50} value was calculated using the linear regression equation obtained from the relationship between the percentage of larval mortality (y) and the log dose (x), namely y = 52.032x - 63.148, where y is the percentage of 50% mortality. This gave an LC_{50} of 143 ppm, which means that at this concentration the extract caused the death of 50% of the larval population within 72 hours. This indicates that the methanol extract of dragon scale fern is toxic and has significant larvicidal activity against *Culex sp*. mosquito larvae.

Figure 5. also shows the correlation coefficient (R^2) = 0.9774 (close to 1) which explains that the relationship between log dose and percentage larval mortality is very strong, which means that this regression model is able to explain about 97.74% of the variation in mortality data observed based on the dose given. The higher the concentration of methanol extract of dragon scale fern leaves, the higher the mortality of *Culex sp*. mosquito larvae, which means the extract is effective as a larvicide.

Bioactive compounds found in plants play a role in killing mosquito larvae; flavonoid compounds work by entering the mosquito's respiratory tract and causing the mosquito's nerves and respiratory muscles to wither so that the mosquito cannot breathe and eventually dies. Saponin compounds work by irritating the lining of the larvae's digestive tract. Saponins also have a bitter effect on the larvae, damaging the waxy layer that protects the insect's outer body, causing the insect to lose a lot of fluid in its body and leading to death. Tannin compounds cause a decrease in the activity of protease enzymes in the

conversion of amino acids. The process of cellular metabolism in the larvae can be disrupted, so the larvae will lack nutrients. In addition, tannins will bind to proteins in the digestive system that the larvae need for growth. If this continues, the larvae will die. The steroid content also affects the larvae, inhibiting the molting process when ingested (Melita, Elsyana and Ulfa, 2022). Steroid compounds are also one of the causes of death in *Culex sp*. mosquito larvae, because steroid compounds are molting inhibitors of mosquito larvae, which cause inhibition of larval development due to failure of metamorphosis of *Culex sp*. mosquito larvae (Ratnawati, Manaf and Sari, 2016).

3.4 Results of Oviposition Deterrent Activity Test of Culex sp. Mosquitoes

The results of the *oviposition deterrent* test of the methanol extract of the leaves of dragon scale fern (*P. piloselloides* (L.) M. G. Price) against *Culex sp*. mosquitoes compared with the activity of abate (positive control) are given in Table 4.4. *Oviposition Deterrent* activity is determined using the % ER parameter to measure the effectiveness of a substance or material in repelling specific insects or organisms. In addition, the OAI is used as a parameter to measure the preference of female insects to lay eggs on a particular extract. Both parameters were determined from the number of *Culex sp*. mosquito eggs at each test concentration. The data are presented in Table 4.

Based on Table 4 above, each concentration of methanol extract has a different effect on the number of eggs laid. At higher concentrations, the number of eggs laid is lower because the effect of the active compounds in the extract is greater, so the activity is stronger, but it will not always be linear. Optimum concentration will have the most significant effect.

The % ER is a metric used to assess a substance's ability, particularly a chemical compound or natural extract, to deter insects from a specific source. This measure evaluates the effectiveness of repellents by calculating the percentage reduction in egg-laying activity due to the extract. Factors influencing % ER include the type of compound, its concentration, volatility, and the insect species involved (sabila, Rahadian and Hidayat, 2013).

OAI is another parameter used to evaluate the preference or avoidance of female insects, such as mosquitoes, for egg-laying sites. The OAI value ranges from -1 to 1, where a value less than 0 indicates a repellent effect, a value greater than 0 indicates an attractant effect, and a value of 0 signifies no significant impact, either as a repellent or attractant.

The percentage values of % ER and OAI of the *oviposition deterrent* activity of methanol extract against the negative control can be seen in Table 5.

Table 5 shows that the methanol extract of the leaves of the dragon scale fern has a strong effect on reducing the number of eggs laid by female *Culex* mosquitoes, with % ER values reaching 72% at a concentration of 2000 ppm.

Table 4. Number of *Culex sp*. Mosquito Eggs in the *Oviposition Deterrent* Activity Test of Dragon Scale Fern Leaf Methanol Extract.

Sample	Number of *Culex sp*. Mosquito Eggs (items)								
	Sample concentration (ppm)							Positive Control	Negative Control
	2000	1000	500	250	125	62.50	31.25		
Methanol extract	7	10	10	14	8	8	12	0	25

Information: - positive control: aquadest + abate; - negative control: aquadest

This percentage indicates that 72% of the female mosquitoes avoided the container

containing the sample extract to lay eggs, which means that the egg-laying inhibitory effect is very significant at high concentrations. Dragon scale fern extract had anti-oviposition effect on female *Culex sp*. mosquitoes at all concentrations (31.25; 62.50; 125; 250; 500; 1000; and 2000 ppm) with OAI values of -0.35; -0.51; -0.51; -0.28; -0.43; -0.43; and -0.56, respectively.

Table 5. Results of Analysis of *Oviposition Deterrent* Activity of Methanol Extract of Dragon Scale Fern Leaves against *Culex sp*. mosquitoes.

Concentration (ppm)	Number of Eggs		ER (%)	OAI
	NC	NT		
2000	25	7	72	-0.56
1000		10	60	-0.43
500		10	60	-0.43
250		14	44	-0.28
125		8	68	-0.51
62.50		8	68	-0.51
31.25		12	52	-0.35

Chakraborty, Burman and Chandra (2022) reported that the chloroform-methanol extract of *Callosobruchus chinensis* seed coat at a concentration of 500 ppm resulted in 79% inhibition of egg laying in *Culex quinquefasciatus* mosquitoes, whereas the results of the larvicidal test against *Culex sp*. mosquitoes in the present study showed 60% inhibition of egg laying at a concentration of 500 ppm. This is because chloroform-methanol extracts often have a higher percent %ER than pure methanol extracts because they can dissolve a wider range of bioactive compounds. Differences in mosquito species can also cause variations in response to certain compounds.

In addition, Chakraborty, Burman and Chandra (2022) reported the OAI value with a result of -0.66 at a concentration of 500 ppm, indicating that the concentration has a repellent effect on *C. quinquefasciatus* mosquitoes. While the calculation of the OAI value at a concentration of 500 ppm in this study is -0.43, which shows that the dragon scale fern extract has a repellent effect on *Culex sp*. This may be caused by the different content of secondary metabolites in the two extracts. The compounds contained in the *C. chinensis* seed coat extract are alkaloids, terpenoids, phenolics, flavonoids, tannins and phytosterols, while the dragon scale fern extract contains only 4 compounds, which is the reason why the OAI value is different even though the concentration is the same.

Flavonoids are believed to act on mosquito eggs by penetrating the eggshell through polygonal pores, leading to structural damage. Similarly, saponins are thought to affect *Culex sp*. mosquito eggs by disrupting the egg wall structure, altering cell wall permeability, and causing fluid loss from the cell, ultimately resulting in dehydration (Madona *et al.*, 2020). Additionally, tannins and steroids are compounds known to actively deter oviposition due to their repellent properties.

The negative control used in the study was aquadest. Based on Table 5 it can be seen that the number of mosquito eggs found in the negative control is higher than the number of eggs found in the methanol extract of dragon scale fern leaves. This is because the methanol extract contains active compounds that make the environment unattractive or uncomfortable for female mosquitoes to lay eggs. In contrast, aquadest, the negative control, did not contain any inhibitory compounds, so female mosquitoes tend to choose aquadest as a safer place to lay their eggs. The extract of dragon scale fern leaves also has a different aroma and taste compared to aquadest. The aroma or taste of the active compounds in dragon scale fern leaves can act as a natural repellent for female

mosquitoes, so they avoid laying eggs in water containing the extract (Abbas *et al.*, 2024).

Based on the results of the study, dragon scale fern extract showed effective larvicidal and *oviposition deterrent* activity against *Culex sp*. This is due to the presence of active compounds such as steroids, saponins, flavonoids and tannins. The combination of the four compounds provides an optimal effect in larvicidal and *oviposition deterrent* activity.

4. CONCLUSIONS

Based on the results of this study, it can be concluded as follows:

1. Secondary metabolite compounds contained in the extract of dragon scale fern (*P. piloselloides* (L.) M. G. Price) are steroid, saponin, flavonoid, and tannin compounds
2. Larvicidal activity of methanol extract of dragon scale fern (*P. piloselloides* (L.) M. G. Price) which is effective against the death of *Culex sp*. larvae obtained an LC_{50} value of 143 ppm
3. Strong *oviposition deterrent* activity of methanol extract of dragon scale fern (*P. piloselloides* (L.) M. G. Price) against *Culex sp*. mosquitoes is found at a concentration of 2000 ppm with an % ER of 72% and at a concentration of 2000 ppm with an OAI value of -0.56.

ACKNOWLEDGMENT

The author would like to thank the Samudra University for the technical supports.

LIST OF REFERENCES

Abbas, M.G., Azeem, M., Bashir, M., Ali, F., Mozuratis, R., and Binyameen, M. (2024) 'Chemical Composition, Repellent, and Oviposition Deterrent Potential of Wild Plant Essential Oils against Three Mosquito Species', *Molecules*, 29(11), p. 2657. Available at: https://doi.org/10.3390/molecules29112657.

Arifin, B., Nasution, R. and Halimatussakdiah (2012) 'Uji Aktivitas Larvasida dan Oviposition deterrent Ekstrak Metanol Daun Vitex trifolia terhadap Nyamuk *Culex*.', *Mataram*, pp. 622–630.

Asiandu, A.P., Widjajanti, H. and Nurnawati, E. (2019) 'Exploration of Endophytic Fungi of Dragon Scale's Fern (Pyrrosia piloselloides (L.) M.G. Price) as an Antibacterial Sources', *BIOVALENTIA: Biological Research Journal*, 5(2). Available at: https://doi.org/10.24233/BIOV.5.2.2019.149.

Chakraborty, S., Burman, S. and Chandra, G. (2022) 'Repellent and oviposition-deterrent efficacies of Cuscuta chinensis on filarial vector Culex quinquefasciatus', *International Journal of Mosquito Research*, 9(3), pp. 48–52. Available at: https://doi.org/10.22271/23487941.2022.v9.i3a.614.

Deti Andasari, S., Hermanto, A.A. and Wahyuningsih, A. (2020) *Perbandingan Hasil Skrining Fitokimia Daun Melinjo (Gnetum gnemon L.) Dengan Metode Maserasi Dan Sokhletasi*, *Jurnal Ilmu Farmasi*.

Edi Kamal, S., Prayitno, S. and Hamdi, S. (2021) 'Antipyretic Effectiveness Test from Dragon (Pyrosia piloselloides) (L) M. G. Price) Leaves Extract in Male Marmutes (Cavia Procellus)', *Jurnal Farmasi Sandi Karsa*, 7(1), pp. 8–14. Available at: https://doi.org/10.36060/jfs.v7i1.77.

Halimatussakdiah, H., Amna, U. and Wahyuningsih, P. (2018) 'Preliminary Phytochemical Analysis and Larvicidal Activity of Edible Fern (Diplazium esculentum (Retz.) Sw.) Extract Against

Culex', *Jurnal Natural*, 18(3), pp. 141–147. Available at: https://doi.org/10.24815/jn.v18i3.11335.

Hestiningsih, R., Giovanny, P.E., Mawarni, A., and Purwantisari, S. (2019) 'Desa Sukodono adalah salah satu wilayah di Kabupaten Demak yang endemik filariasis (angka rata-rata 1,39%). Penemuan kasus baru dan mikrofilaria pada tubuh penderita kronis meningkatkan potensi terjadinya penularan dan infeksi mikrofilaria pada nyamuk. Pe', *Jurnal Ilmiah Permas: Jurnal Ilmiah STIKES Kendal*, 9(2), pp. 165–174. Available at: https://doi.org/10.32583/pskm.9.2.2019.165-174.

Kalaimurgan, D., Lalitha, K., Govindarajan, R., Unban, K., Shivakumar, M., Venkatesan, S., Khanongnuch, C., Husain, F., Qais, F., Hasan, I., Karuppiah, P., Khan, A., and Adil, M. (2023) 'Biogenic synthesis of zinc oxide nanoparticles using Drynaria Quercifolia tuber extract for antioxidant, antibiofilm, larvicidal, and photocatalytic applications', *Biomass Conversion and Biorefinery* [Preprint]. Available at: https://doi.org/10.1007/s13399-023-04751-3.

Kusnadi, and Devi, E.T. (2017) *Isolasi dan Identifikasi Senyawa Flavonoid pada Ekstrak Daun Seledri (Apium graveolens L.) dengan Metode Refluks*. Available at: http://e-journal.ups.ac.id/index.php/psej.

Madona, M., Setyaningrum, E., Pratami, G., and Kanedi, M. (2020) *Efektivitas Ekstrak Daun Tomat (Solanum lycopersicum L.) sebagai Ovisida Nyamuk Aedes aegypti*, *Jurnal Ilmu Kedokteran Dan Kesehatan*.

Manongko, P.S., Sangi, M.S. and Momuat, L.I. (2020) 'Uji Senyawa Fitokimia dan Aktivitas Antioksidan Tanaman Patah Tulang (Euphorbia tirucalli L.)', *Jurnal MIPA*, 9(2), p. 64. Available at: https://doi.org/10.35799/jmuo.9.2.2020.28725.

Ekayani, M., Juliantoni, Y., and Hakim, A. (2021) 'Uji Efektivitas Larvasida dan Evaluasi Sifat Fisik Sediaan Losio Antinyamuk Ekstrak Etanol Daun Kirinyuh (Chromolaena odorata L.) terhadap Nyamuk Aedes Aegypti', 2(4).

Marlina, S.D., Suryati, V. and Suyono, S. (2005) 'The phytochemical screenings and thin layer chromatography analysis of chemical compounds in ethanol extract of labu siam fruit (Sechium edule Jacq. Swartz.)', *Biofarmasi Journal of Natural Product Biochemistry*, 3(1), pp. 26–31. Available at: https://doi.org/10.13057/biofar/f030106.

Melita, D.A., Elsyana, V. and Ulfa, A.M. (2022) *Indonesian Journal of Biological Pharmacy Effectiveness of Papaya Leaf (Carica papaya L.) Extraxt As A Larvicide of Aedes aegypti Mosquito Efektivitas Ekstrak Etil Asetat Daun Pepaya (Carica papaya L.) Sebagai Larvasida Nyamuk Aedes aegypti*.

Nola, F., Putri, G. K., Malik. L. H., and Andriani.N. (2021) 'Isolasi Senyawa Metabolit Sekunder Steroid dan Terpenoid dari 5 Tanaman', *Syntax Idea*, 3(7), pp. 1612–1619. Available at: https://doi.org/10.46799/syntax-idea.v3i7.1307.

Nurjannah, I., Ayu, B., Mustariani, A., and Suryani, N. (2022) 'Skrining Fitokimia dan Uji Antibakteri Ekstrak Kombinasi Daun Jeruk Purut (Citrus hystrix) dan Kelor (Moringa oleifera L.) sebagai Zat Aktif pada Sabun Antibakteri', *SPIN*,

4(1), pp. 23–36. Available at: https://doi.org/10.20414/spin.v4i1.4801.

Putri Anggraeni, P., Chatri, M. and Advinda, L. (2023) *Characteristics of Saponin Secondary Metabolite Compounds in Plants Karakteristik Saponin Senyawa Metabolit Sekunder pada Tumbuhan*.

Ratnawati, D., Manaf, S. and Sari, Y.N. (2016) 'Aktivitas Larvasida Ekstrak Metanol Daun Selasih (*Ocimum basilicum*) Terhadap Larva Nyamuk *Aedes aegypti'*, *Jurnal Gradien*, 12(2), pp. 1181–1186.

Reegan, A.D. *et al.* (2015) 'Ovicidal and Oviposition Deterrent Activities of Medicinal Plant Extracts Against Aedes aegypti L. and Culex quinquefasciatus Say Mosquitoes (Diptera: Culicidae)', *Osong Public Health and Research Perspectives*, 6(1), pp. 64–69. Available at: https://doi.org/10.1016/j.phrp.2014.08.009.

sabila, M.F., Rahadian, R. and Hidayat, J.W. (2013) 'Preferensi Peletakan Telur dan Penghambatan Perkembangan Pra Dewasa Nyamuk Aedes aegypti L. di Berbagai Media Air', *Jurnal Biologi*, 2(4), pp. 45–53.

Santos, N., Albuquerque, L., de Amorim, M.., de Oliveira, S.J., Pracopio, T., Santos, P., Paiva, P., Barros, M., Napoleao, T., and Pontual, E. (2023) 'Effects of Lectin Preparations from Microgramma vacciniifolia Rhizomes on the Survival, Digestive Enzymes, and Acetylcholinesterase Activity of Alphitobius diaperinus (Panzer) (Coleoptera: Tenebrionidae)', *Macromol*, 3(3), pp. 451–462. Available at: https://doi.org/10.3390/macromol3030027.

Shukla, S. (2011) 'Insecticidal Acti Insecticidal Activity of Vity of Dryopteris Filix-mas (LINN.) (LINN.) schott (LINN.) Ethanolic Extract Against Corcyra Cephalonica Staint. (Lepidoptera: Pyralidae)', *Journal of Biopesticides*, 04(02), pp. 138–143. Available at: https://doi.org/10.57182/jbiopestic.4.2.138-143.

Sukaeningsih, D., Sukandar, E.Y. and Qowiyyah, A. (2021) 'Tanaman Famili Fabaceae yang Berpotensi sebagai Obat Herbal Antitukak Peptik', *Jurnal Sains dan Kesehatan*, 3(3), pp. 356–365. Available at: https://doi.org/10.25026/jsk.v3i3.296.

Sumihe, G., Runtuwene, M.R.J. and Rorong, J.A. (2014) 'Analisis Fitokimia dan Penentuan Nilai LC_{50} dan Ekstrak Metanol Daun Liwas', *Jurnal Ilmiah Sains*, 14(2). Available at: https://doi.org/10.35799/jis.14.2.2014.6070.

Tutik, T. and Marcellia, S. (2021) 'Uji Efektivitas Larvasida Ekstrak Kulit Bawang Merah (Allium cepa L.) terhadap Larva Aedes aegypti', *Jurnal Farmasi Malahayati*, 3(2), pp. 148–158. Available at: https://doi.org/10.33024/jfm.v3i2.3445.

Vifta, R.L. and Advistasari, Y.D. (2018) 'Skrining Fitokimia, Karakterisasi, dan Penentuan Kadar Flavonoid Total Ekstrak dan Fraksi-Fraksi Buah Parijoto (Medinilla speciosa B.) Pytochemical Screening, Characterization, and Determination of Total Flavonoids Extracts and Fractions of Parijoto Fruit (Medinilla speciosa B.)', *Prosiding Seminar Nasional Unimus*, 1.

Yuliana, A. Rinaldi, R., Rahayuningsih, N.,

and Gustaman, F. (2021) 'Efektivitas Larvasida Granul Ekstrak Etanol Daun Pisang Nangka (Musa x paradisiaca L.) terhadap Larva Nyamuk Aedes aegypti', *ASPIRATOR - Journal of Vector-borne Disease Studies*, 13(1), pp. 69–78. Available at: https://doi.org/10.22435/asp.v13i1.4042.

Jurnal Ilmiah Berkala: Sains dan Terapan Kimia
Vol. 19 No. 2, Juli 2025

Fluorescent Silica Nanofertilizer for Enhancement of Photosynthesis Rate

Nanofertilizer Silika Fluoresens untuk Peningkatan Laju Fotosintesis

Fransiskus Hottua Malau[1)], Carlos Rewandesno Sitorus[1)], Pebry Asarona Sianipar[1)], Winri Imanuela Sihombing[1)], Nurul Pratiwi Santoso[1)], Lisnawaty Simatupang[1)*]

[1]Jurusan Kimia, Fakultas Matematika dan Ilmu Pengetahuan Alam, Universitas Negeri Medan, Jl. Willem Iskandar Psr. V, Medan, 20221, Sumatera Utara, Indonesia

*Email: lisnawaty@unimed.ac.id

ABSTRACT

This study aims to synthesize and characterize fluorescent silica nanofertilizers using Mount Sinabung volcanic ash as a silica source. The synthesis method involved extracting silica from ash using a concentrated acid solution, followed by functionalization using triethanolamine (TEA) via the sol-gel method. Characterization included surface morphology analysis using Scanning Electron Microscopy (SEM), crystal structure identification using X-ray Diffraction (XRD), functional group identification using Fourier Transform Infrared (FTIR), and UV absorption measurement using UV-Vis Spectroscopy. The results showed that fluorescent silica nanofertilizers exhibited smooth surface morphology, uniform particle size distribution (particle size: 48.49 ± 1.31 nm), amorphous structure with increased crystallinity after TEA functionalization (crystallinity: 11.88%), and significant enhancement in UV absorption (absorbance: 0.65) and fluorescence after TEA functionalization. The conclusion of this study is that fluorescent silica nanofertilizers can enhance plant photosynthesis efficiency through improved light absorption and fluorescence properties.

Keywords: Sinabung ash, silica, fluorescent silica nanofertilizer, photosynthesis rate.

ABSTRAK

Paku sisik naga (Pyrrosia piloselloides (L.) M. G. Price) adalah salah satu tumbuhan yang tumbuh dan Penelitian ini bertujuan untuk mensintesis dan mengkarakterisasi nanofertilizer silika fluoresens dengan memanfaatkan abu Gunung Sinabung sebagai sumber silika. Metode sintesis melibatkan ekstraksi silika dari abu menggunakan larutan asam pekat, diikuti dengan fungsionalisasi menggunakan trietanolamin (TEA) melalui metode sol-gel. Karakterisasi meliputi analisis morfologi permukaan dengan Scanning Electron Microscopy (SEM), identifikasi struktur kristal dengan X-ray Diffraction (XRD), pengidentifikasian gugus fungsi dengan Fourier Transform Infrared (FTIR), dan pengukuran penyerapan UV menggunakan UV-Vis Spectroscopy. Hasil penelitian menunjukkan bahwa nanofertilizer silika fluoresens memiliki morfologi permukaan yang halus dan distribusi ukuran partikel yang seragam (ukuran partikel: 48,49 ± 1,31 nm), struktur amorf dengan peningkatan kristalinitas setelah fungsionalisasi TEA (kristalinitas: 11,88%), serta peningkatan signifikan dalam penyerapan UV (absorbansi: 0,65) dan fluoresensinya setelah fungsionalisasi dengan TEA. Kesimpulan dari penelitian ini adalah nanofertilizer silika fluoresens dapat meningkatkan efisiensi fotosintesis tanaman melalui sifat penyerapan cahaya dan fluoresensi yang ditingkatkan..

Kata Kunci : Abu sinabung, silika, nanofertilizer silika fluoresens, laju fotosintesis.

Received: 01 January 2025 ; **Accepted**: 26 July 2025: **Available online**: 30 July 2025

---

1. INTRODUCTION

Agricultural productivity is a critical issue, especially given its impact on global food security. Rapid global population growth exacerbates these productivity constraints, demanding increased efficiency and innovation in agricultural practices (Chugh et al., 2021). Unpredictable climate change, including rising temperatures and changing weather patterns, also affects the intensity of sunlight received by plants, which in turn influences the rate of photosynthesis (Dilnawaz et al., 2023). Moore et al. (2021) have studied the interaction of leaves with rising temperatures and heat stress, which can disrupt the rate of photosynthesis and plant development. High photosynthetic efficiency is crucial for agricultural productivity, and innovative and environmentally friendly technologies are key to achieving this goal sustainably (Dilnawaz et al., 2023).

Excessive use of chemical fertilizers has been shown to damage soil health, the environment, waterways, and reduce farmers' profits (Chugh et al., 2021). Silica nanoparticles with flexible properties and good biocompatibility have been widely used in various biological applications. The ability to combine siloxane precursors with fluorescent dyes in silica nanoparticles enables the engineering of nanomaterials for various fields (Gubala et al., 2020). Nano technology is considered to have great potential for developing innovative products in various aspects, including agriculture (FAO and WHO, 2013). The development of nano technology in Indonesia is still relatively new (Rahayu, 2021). Nano technology is expected to be a solution to improve fertilization efficiency, reduce environmental impact, and optimize plant growth (Li et al., 2023).

Research shows that volcanic ash from Mount Sinabung contains 51.8% silica (SiO2) in the form of nanoparticles, which have the potential to be used as nanofertilizers (Bariyah and Simatupang, 2020). Silica nanoparticles offer a promising alternative with a large surface area, enabling them to increase the efficiency of nutrient absorption by plants. The use of nanotechnology in agriculture can stimulate plant growth and enhance disease resistance, as well as improve agricultural productivity through smart and environmentally friendly nutrient release patterns (Chugh et al., 2021; Du et al., 2022).

Silica nanoparticles (SiNPs) have unique properties, including a large surface area, penetration capability, and a structure that allows them to penetrate plants and regulate their metabolic processes (Goswami et al., 2022). Previous research has demonstrated the potential of fluorescent silica nanoparticles derived from coal fly ash as a sustainable and environmentally friendly raw material (Singh et al., 2024). Functionalization with polar groups using the hydrothermal method enhances nanoparticle stability and dispersion, enabling more effective applications (Saita and Kawasaki, 2021). The use of SiNPs as nano-fertilizers helps protect plants against pathogens in leaf tissues and supports increased photosynthesis rates through the transfer of energy emission to chlorophyll (Li et al., 2020).

The significance of this research lies in its innovation in utilizing abundant local natural resources, namely volcanic ash from Mount Sinabung, which has the potential to become a sustainable solution to global agricultural problems. This research aims to develop fluorescent silica nanoparticles from Mount Sinabung geomaterials with modified amino groups to enhance the stability and dispersion of the nanoparticles as a nanofertilizer. The benefits of this research include improved fertilization efficiency, reduced environmental impact from the use of chemical fertilizers, and increased crop productivity through optimized photosynthesis rates.

2. MATERIALS AND METHODS

2.1. Materials

The main materials used in this study were volcanic ash from Mount Sinabung obtained from Namanteran Village, Kabanjahe Regency, sodium hydroxide (NaOH) e-merck, hydrochloric acid (HCl 37%) e-merck, triethanolamine (TEA), ethanol pro analys, and distilled water (H_2O).

2.2. Methods

In this study, the sol-gel method was used for the synthesis of silica and fluorescent silica. The method used refers to the research by Bariyah and Simatupang (2020) and Singh et al (2024) with the following modifications.

2.2.1. Synthesis of Silica from Sinabung Ash

Twenty grams of 200-mesh ash sample were added to a 12 M HCl solution for 24 hours. The volcanic ash was then neutralized with distilled water and dried at 120 °C for 6 hours. After weighing, the Sinabung ash was added to 8 M NaOH and boiled until thickened. The solution was then placed in a furnace at 750 °C for 3 hours, cooled, and mixed with 200 mL of distilled water before being left to stand overnight. The mixture was filtered, and the resulting solution was titrated with 3M HCl while stirring with a magnetic stirrer at 40 °C until the pH approached 7. The precipitate formed was then filtered, washed with distilled water, and dried at 120 °C for approximately 3 hours.

2.2.2. Synthesis of Fluorescent Silica Nanofertilizer

Silica nanoparticles (in variations of 0.5 g, 1.0 g, and 1.5 g) were dissolved in 25 mL of ethanol at a temperature of 40 °C for 30 minutes. Five milliliters of TEA were slowly added while stirring at a temperature of 60 °C for 2 hours. After the reaction was complete, the mixture was cooled and centrifuged at 10,000 rpm for 10 minutes to obtain the amine-modified fluorescent silica nanofertilizer supernatant. The resulting nanofertilizer was then dried at 50 °C, dissolved into a stock solution, and stored at 4°C for further use.

2.2.3. Characterization of Silica and Fluorescent Silica

Morphological and particle size analysis was performed using a Scanning Electron Microscope (SEM) to determine the size distribution and particle shape at various magnifications. Crystallinity or amorphous structure determination was performed using X-Ray Diffraction (XRD) to identify crystalline phases and crystallinity degree. Fluorescence absorption spectra were measured using a UV-Vis spectrophotometer, and functional groups were identified using Fourier Transform Infrared (FTIR) Spectroscopy.

3. RESULTS AND DISCUSSION

3.1 Extraction of Silica from Sinabung Ash

Silica found in nature is impure, so to obtain silica in a material, separation and purification from other elements contained in the sample must be carried out. To obtain pure silica from Sinabung ash, extraction was performed using concentrated HCl 37% (12 M) to dissolve impurity metals such as Fe, Ca, Al, and other metals from the ash sample. After the purification process, 18 grams of ash were obtained from the 20 grams of sample used.

Next, sodium silicate as a silica precursor was made by adding 8 M NaOH to the activated ash. This reaction produced a sodium silicate (Na_2SiO_3) solution, which was then reacted with 3 M HCl to precipitate silica as a stable white gel.

Silica was successfully synthesized from Mount Sinabung ash using the sol-gel method, yielding 9.015 grams of silica with a yield of 49.78% w/w (Figure 1). The yield obtained was quite high and consistent with literature stating that the silica content in Mount Sinabung ash is 51.8%. Sinabung ash has advantages over other raw materials because, in addition to its abundant availability, it was initially considered merely air pollution but

can now be utilized to produce more beneficial silica.

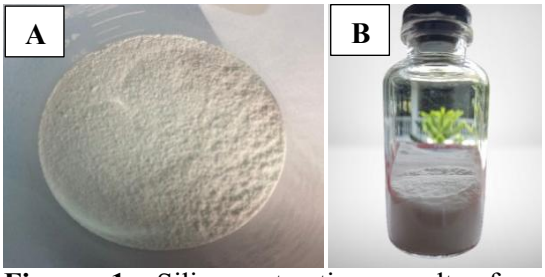

Figure 1. Silica extraction results from Sinabung volcanic ash

3.2 Silica Characterization Results

3.2.1. Silica Particle Morphology and Size

The surface morphology and particle size of silica were characterized using Scanning Electron Microscopy (SEM). The SEM image (Figure 2.a) shows silica particles with a regular and homogeneous morphology. The average silica particle size is approximately 58.80 ± 1.14 nm (Figure 2.b), with a uniform size distribution. These observations indicate that the sol-gel method is effective in producing silica particles with an ideal size for agricultural nanotechnology applications, which are important as precursors to produce nanofertilizers.

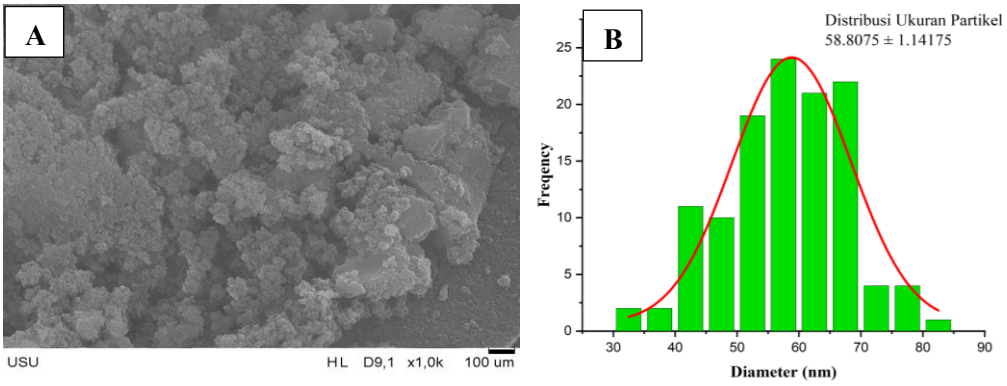

Figure 2. (a) Morphology of silica particles synthesized using SEM, (b) Size distribution of silica particles.

3.2.2. Crystal Structure and Amorphousness

Analysis using X-ray Diffraction (XRD) shows that the produced silica has an amorphous structure. In the XRD pattern (Figure 3.a), a broad diffraction peak (halo) is observed at an angle of 2θ around 22°, which is characteristic of amorphous materials. The low regularity in atomic spacing confirms that this silica does not have a regular crystalline structure. This is consistent with the characteristics of silica produced from volcanic ash, which tends to have an amorphous structure rather than a crystalline one (Nelson, 2018).

3.2.3. Functionality Analysis with FTIR

The results of characterization using Fourier Transform Infrared Spectroscopy (FTIR) show a spectrum characteristic of silica. Figure 3.b shows the presence of a Si-O-Si stretching band at 1085 cm^{-1}, indicating strong bonds between silicon and oxygen atoms in the siloxane structure. The peak at 810 cm^{-1} indicates Si-OH bending, signifying the presence of hydroxyl groups. The band at 460 cm^{-1} reinforces the presence of Si-O bonds in the silica structure. The FTIR spectrum also shows a broad band in the 3200–3600 cm^{-1} range, indicating surface hydration of silica, as well as a peak at 1640 cm^{-1} indicating the presence of adsorbed water on the silica surface (Usgodaarachchi et al., 2021).

This analysis confirms that silica produced from Sinabung ash has the appropriate functional groups for application as a nanofertilizer.

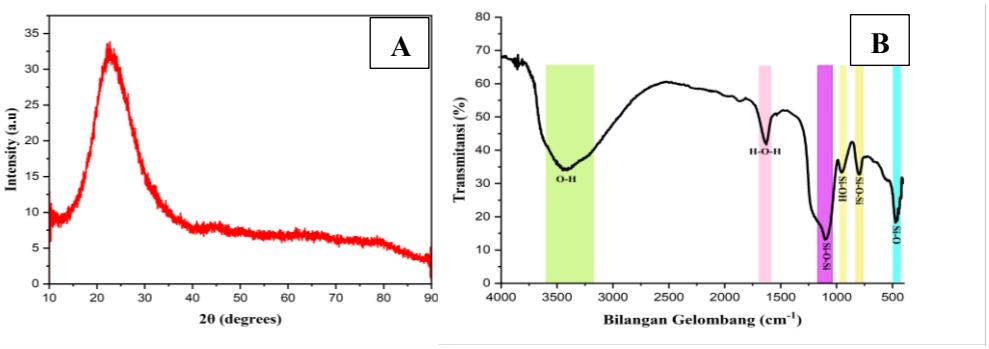

Figure 3. (a) XRD spectrum of silica with an amorphous structure, (b) FTIR spectrum of silica with specific peaks for siloxane and silanol groups.

Figure 4. (a) Silica functionalization process with triethanolamine, (b) Grinding of the synthesized fluorescent silica, and (c) Fluorescent silica variants 1, 2, and 3 that have been ground.

3.3. Synthesis of Fluorescent Silica Nanofertilizer

The synthesis of fluorescent silica nanofertilizer was carried out using the sol-gel method to ensure purity and uniform particle size distribution. Each variant of the nanofertilizer uses different silica concentrations (0.5 g, 1.0 g, 1.5 g) dissolved in ethanol as the solvent. Triethanolamine (TEA) is used as an amine functionalization agent to modify the silica surface.

Silica functionalization with TEA aims to enhance fluorescence and UV absorption properties. This process is illustrated in Figure 4.a, where silica is reacted with TEA at a controlled temperature. After the functionalization process is complete, the resulting product is then ground to ensure uniform size, as shown in Figure 4.b. The final product consists of fluorescent silica in three different variants, as shown in Figure 4.c.

The functionalization process using TEA is important because the amino groups bound to the silica surface can enhance the stability and dispersibility of nanoparticles in solutions, as well as improve interactions between nanoparticles and plants. TEA also aids in the formation of a more ordered structure on the silica surface, contributing to improved efficiency in UV light absorption and fluorescence.

3.4. Results of Fluorescent Silica Characterization

FTIR spectroscopy was used to confirm the success of the amine functionalization process on silica. In Figure 5.a, the presence of N–H stretching bands in the 3300–3500 cm^{-1} range and N–H bending bands in the 1500–1650 cm^{-1} range indicates that the amine groups were successfully bound to the silica surface. Additionally, there is a C–H stretching band in the 2800–3000 cm^{-1} range originating from the methylene ($–CH_2$) and methyl ($–CH_3$) groups of triethanolamine (TEA). The

intensity of these bands varies according to the ratio of silica and TEA concentrations used, with variant 1 showing the clearest intensity, indicating a higher degree of functionalization.

the morphology and particle size of silica. A uniform particle size distribution is crucial in nanofertilizer applications as it ensures consistent absorption by plants, thereby enhancing nutrient utilization efficiency.

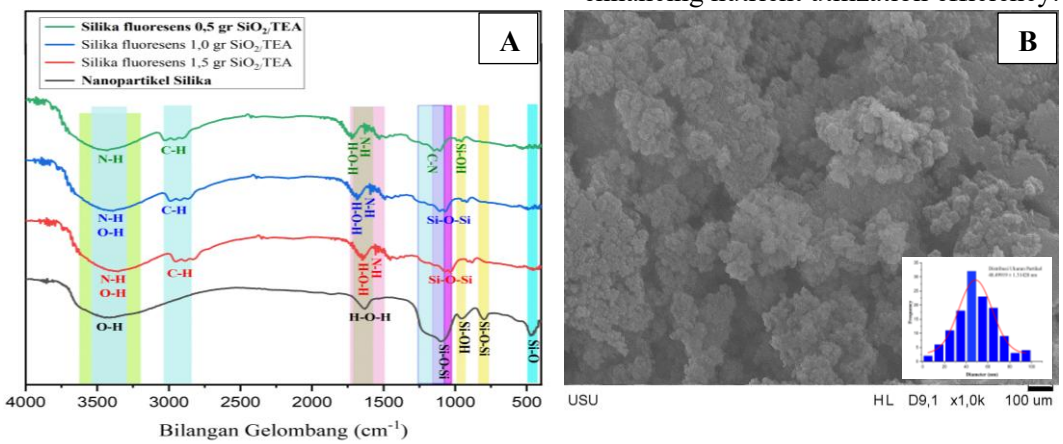

Figure 5. (a) FTIR spectrum of fluorescent silica nanofertilizer variants 1, 2, 3, and silica (b) Surface morphology of fluorescent silica nanofertilizer variant 1

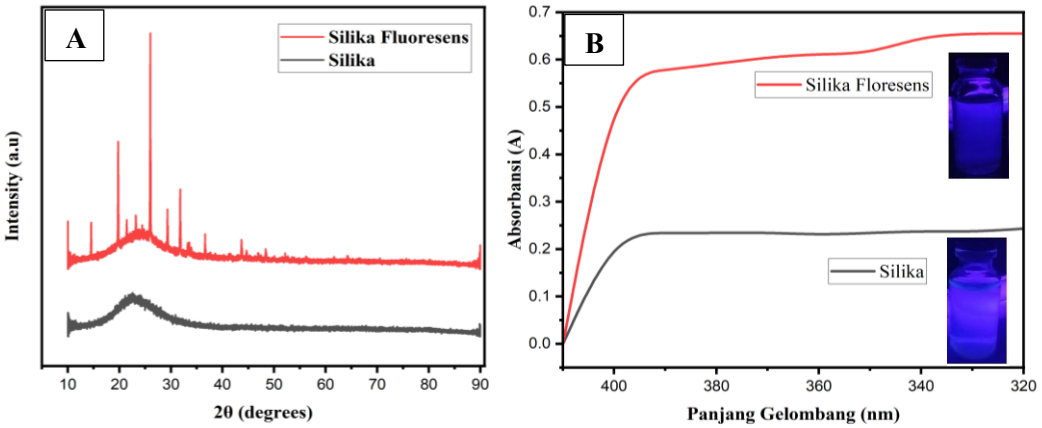

Figure 6. (a) XRD diffraction pattern of fluorescent silica nanofertilizer and (b) increased absorbance spectrum of fluorescent silica nanofertilizer.

Analysis using Scanning Electron Microscopy (SEM) in Figure 5.b shows that modification of silica with TEA results in a smoother surface morphology and more uniform particle size distribution compared to the initial silica. The particle size of the fluorescent silica nanofertilizer is also smaller, approximately 48.49 ± 1.31 nm, and more uniform. This indicates that the functionalization process not only improves the surface chemical properties but also affects

The X-ray Diffraction (XRD) pattern in Figure 6.a indicates an increase in silica crystallinity after modification with TEA. The initial silica had an amorphous structure with crystallinity of approximately 0.87%.

After modification, crystallinity increased to 11.88% with crystal size of approximately 52.01 ± 1.02 nm. TEA helps rearrange the atomic structure within the silica, thereby enhancing crystallinity and improving the resulting material structure.

This increase in crystallinity is important as it enhances the thermal and mechanical stability of the nanofertilizer, making it more resistant to varying environmental conditions when applied to plants.

Figure 6.b shows the increase in absorbance values using UV-Vis spectrophotometry in the UV-A wavelength range (320–400 nm). The absorbance value increased from 0.23 for the initial silica to 0.65 for the fluorescent silica nanofertilizer. This increase in absorbance indicates that the fluorescent silica nanofertilizer is more effective in absorbing UV light. Fluorescence observations under UV light also show that the fluorescent silica nanofertilizer emits a clearer blue light compared to the initial silica. The increased intensity of blue light emission indicates that the fluorescent silica nanofertilizer has better fluorescent properties, which could enhance plant photosynthetic activity by utilizing absorbed UV light and converting it into more effective blue light for plant use.

Overall, the characterization results indicate that the produced fluorescent silica nanofertilizer has superior physical and chemical properties compared to the original silica. The increased crystallinity, uniform particle size distribution, and improved fluorescence properties suggest that this nanofertilizer has significant potential to enhance photosynthetic efficiency and plant growth. The success of the amine functionalization process also indicates that the method used is effective in producing nanofertilizers with desired characteristics. The use of TEA as a functionalization agent has proven to enhance the UV absorption properties and fluorescence capability of silica, making it more beneficial as a nanofertilizer.

This study shows that silica from Mount Sinabung ash, which was initially considered waste, can be processed into a high-value material with significant applications in agriculture. The resulting fluorescent silica nanofertilizer has the potential to improve nutrient use efficiency in plants, reduce dependence on conventional chemical fertilizers, and support more sustainable agriculture.

4. CONCLUSIONS

This study successfully synthesized silica from Mount Sinabung ash using the sol-gel method, yielding silica with a yield of 49.78%. Characterization of the silica revealed an amorphous morphology with a particle size distribution of 58.80 ± 1.14 nm. Furthermore, fluorescent silica nanofertilizer was successfully synthesized using triethanolamine modification, exhibiting a smooth surface morphology and uniform particle size distribution (48.49 ± 1.31 nm). FTIR analysis confirmed the functionalization of amine on the nanofertilizer, while XRD showed an increase in crystallinity from 0.87% to 11.88% after modification. UV-Vis spectrophotometry showed an increase in absorbance and blue fluorescence intensity in the nanofertilizer, indicating its potential to enhance plant photosynthetic activity more effectively.

ACKNOWLEDGMENT

The author would like to thank the Ministry of Education and Culture (Kemdikbud) for funding this research through the 2024 Student Creativity Program in Exact Sciences Research and the State University of Medan for funding the publication of this scientific article.

LIST OF REFERENCES

Bariyah, S. dan Simatupang, L. (2020). Activation of Sinabung Mount Volcanic Ash using Various Mineral Acids. *Indonesian Journal of Chemical Science and Technology (IJCST)*, *4*(1), 1-4. https://doi.org/10.24114/ijcst.v4i1.23087.

Chugh, G., Siddique, K. H. dan Solaiman, Z. M. (2021). Nanobiotechnology for agriculture: smart technology for combating nutrient deficiencies with nanotoxicity challenges. *Sustainability*, *13*(4), 1781. https://doi.org/10.3390/su13041781.

Du, J., Liu, B., Zhao, T., Xu, X., Lin, H., Ji, Y. dan Ding, X. (2022). Silica nanoparticles protect rice against biotic and abiotic stresses. *Journal of Nanobiotechnology*, *20*(1), 1-18. https://doi.org/10.1186/s12951-022-01420-x.

Goswami, P., Mathur, J., & Srivastava, N. (2022). Silica nanoparticles as novel sustainable approach for plant growth and crop protection. *Heliyon* 8 (7). https://doi.org/10.1016/j.heliyon.2022.e09908.

Gubala, V., Giovannini, G., Kunc, F., Monopoli, M. P. dan Moore, C. J. (2020). Dye-doped silica nanoparticles: synthesis, surface chemistry and bioapplications. *Cancer Nanotechnology*, *11*(1), 1-43. https://doi.org/10.1186/s12645-019-0056-x.

Li, D., Li, W., Zhang, H., Zhang, X., Zhuang, J., Liu, Y. dan Lei, B. (2020). Far-red carbon dots as efficient light-harvesting agents for enhanced photosynthesis. *ACS applied materials & interfaces*, *12*(18), 21009-21019. https://dx.doi.org/10.1021/acsami.9b21576.

Li, Y., Xi, K., Liu, X., Han, S., Han, X., Li, G. dan Zhu, Y. (2023). Silica nanoparticles promote wheat growth by mediating hormones and sugar metabolism. *Journal of Nanobiotechnology*, *21*(1), 2. https://doi.org/10.1186/s12951-022-01753-7.

Moore, C. E., Meacham-Hensold, K., Lemonnier, P., Slattery, R. A., Benjamin, C., Bernacchi, C. J. dan Cavanagh, A. P. (2021). The effect of increasing temperature on crop photosynthesis: from enzymes to ecosystems. *Journal of Experimental Botany*, *72*(8), 2822-2844. https://doi.org/10.1093/jxb/erab090.

Nelson, S. A. (2018). *X-Ray Crystallography*. Tulane University. URL: https://translate.google.com/translate?u=https://www2.tulane.edu/~sanelson/eens211/x-ray.htm&hl=id&sl=en&tl=id&client=srp&prev=search.

Rahayu, C. S. (2021). *Artifacts – Teknologi Nano*. URL: https://hmpg.che.itb.ac.id/index.php/2021/08/27/artifacts-teknologi-nano/.

Saita, S. dan Kawasaki, H. (2021). Origin of the fluorescence in silica-based nanoparticles synthesized from aminosilane coupling agents. *Journal of Luminescence*, *232*, 117849. https://doi.org/10.1016/j.jlumin.2020.117849.

Singh, V., Mandal, T., Mishra, S. R., Singh, A. dan Khare, P. (2024). Development of amine-functionalized fluorescent silica nanoparticles from coal fly ash as a sustainable source for nanofertilizer. *Scientific Reports*, *14*(1), 3069. https://doi.org/10.1038/s41598-024-53122-z.

Usgodaarachchi, L., Thambiliyagodage, C., Wijesekera, R., & Bakker, M. G. (2021). Synthesis of mesoporous silica nanoparticles derived from rice husk and surface-controlled amine functionalization for efficient adsorption

of methylene blue from aqueous solution. *Current Research in Green and Sustainable Chemistry*, *4*, 100116. https://doi.org/10.1016/j.crgsc.2021.100116.

Jurnal Ilmiah Berkala: Sains dan Terapan Kimia
Vol. 19 No. 2, Juli 2025

Photocatalytic Degradation of Phenol Red Using Titanium Dioxide (TiO_2)–Chitosan Composite Catalyst Assisted By Solar Energy

Degradasi Fotokatalitik Fenol Merah Menggunakan Katalis Komposit Titanium Dioksida (TiO_2)-Kitosan Dengan Bantuan Energi Sinar Matahari

M. Ridwan Baidhowi[1*], Taufiqur Rohman[1], Utami Irawati[1]

[1]Jurusan Kimia, Fakultas Matematika dan Ilmu Pengetahuan Alam, Universitas Lambung Mangkurat, Jl. Ahmad Yani Km 36 Banjarbaru 70714 Kalimantan Selatan, Indonesia

*Email: ridwanbaidhowi26@gmail.com

ABSTRACT

Phenol Red is a very water-soluble textile dye that belongs to the triphenylmethane dye class. In this study, a photocatalyst composite was synthesized by combining TiO_2 as photocatalyst with chitosan as a solid support material. The aim of this research is to study what ratio of TiO_2: Chitosan would yield the best-performing composites in catalysing the photodegradation of phenol red. This research also studied, the optimum dose of TiO_2-chitosan for photodegradation of phenol red, and the effect of solar radiation time towards the photodegradation of phenol red. Into 100 mL of phenol red solution with an initial concentration of 25 ppm, chitosan beads and TiO_2-Chitosan composites were added with various doses, i.e: 0.5:100, 1:100, 2:100, and 5:100 gram/mL. The mixtures were put into solar radiaton exposure for 6 hours, where the concentration of phenol red in the solution was analysed every 20 minutes. The highest degradation level of phenol red (72.84%) was achieved by using TiO_2-Chitosan 5:10 composites, where the dose added was 5 grams of composite for in 100 mL sample along with a 6-hour of solar radiation exposure.

Keywords: *Phenol red, photochemistry, TiO_2-Chitosan composite, solar radiation*

ABSTRAK

Fenol merah adalah pewarna tekstil yang sangat larut dalam air yang termasuk dalam kelas pewarna triphenylmethane. Dalam penelitian ini, dilakukan pengolahan atas fenol merah menggunakan komposit kitosan. Tujuan dari penelitian ini adalah mendapatkan data rasio TiO_2: Kitosan yang menghasilkan komposit dengan kemampuan paling baik dalam proses fotodegradasi fenol merah, mendapatkan dosis optimum TiO_2-Kitosan yang efektif dalam proses fotodegradasi fenol merah, dan mendapatkan informasi mengenai pengaruh atas waktu penyinaran terhadap fotodegradasi fenol merah. Larutan fenol merah dengan konsentrasi 25 ppm sebanyak 100 mL ditambah dengan beads kitosan dan komposit TiO_2-kitosan sebanyak 0,5:100, 1:100, 2:100, dan 5:100 gram/mL. Larutan disinari dengan sinar matahari selama 6 jam, dimana konsentrasi fenol merah dalam larutan dianalisis setiap 20 menit. Degradasi fenol merah tertinggi (72,84 %) dicapai pada komposit TiO_2-Kitosan 5:10, dimana dosis yang ditambahkan adalah 5 gram komposit dalam 100 mL larutan dengan penyinaran selama 6 jam.

Kata Kunci : *Fenol merah, fotokimia, komposit TiO_2-kitosan, sinar matahari*.

Received: 01 January 2025; **Accepted**: 26 July 2025; **Available online**: 30 July 2025

1. INTRODUCTION

The textile industry is one of the fastest-growing industries and plays an important role in Indonesia. During the production process, this industry generates solid and liquid waste containing various toxic compounds that can pollute the environment if not properly treated. The main pollutants in textile waste originate from the dyeing and finishing processes, which involve both synthetic and natural dyes to produce permanent colors. A key characteristic of textile industry effluents is their high content of synthetic dyes, which, when discharged into the environment, can harm aquatic ecosystems.

Phenol red is a highly water-soluble textile dye belonging to the triphenylmethane class of dyes. At room temperature, phenol red appears as red crystals, is stable in air, and has a solubility of 0.77 g/L in water. At 20°C, the compound has a pKa value of 8.00. Therefore, phenol red is often used as a reagent to measure water pH within the range of pH > 6.8. Its application as an indicator is widely practiced in cell biology laboratories and for water quality testing (Mittal et al., 2009).

The most common method for treating textile waste is adsorption. This process is simple and widely used for removing organic pollutants. However, adsorption has certain limitations, including the need for adsorbent regeneration once it becomes saturated with organic compounds. An effective alternative for treating dye waste, including phenol red, is photocatalysis. Photocatalysis combines photochemical and catalytic processes to enable chemical transformation reactions (Febriyani et al., 2012). Titanium dioxide (TiO_2) is one of the most widely used semiconductor materials that acts as a photocatalyst. Chiou et al. (2008) reported that TiO_2 can degrade phenol by up to 56%. The advantages of TiO_2 photocatalysts include high chemical stability, low cost, and non-toxicity (Hashimoto et al., 2005). Additionally, chitosan is often used alongside TiO_2 due to its excellent ability to adsorb both organic and inorganic pollutants (Aranas et al., 2010).

2. MATERIALS AND METHODS

2.1. Materials

The instrument that was used in this research include Pyrex glassware, a Genesys 10uv UV-Visible Spectrophotometer, SEM (Scanning Electron Microscope), FTIR (Fourier-transform Infrared Spectroscopy), pH meter, magnetic stirrer, irradiation box, glass reactor, Philips UV lamp (30 Watt), Recent RC-999 aerator, Recent RC-650 submersible pump, analytical balance (O'Hauss), and PMC stirrer. The materials used in this study are TiO_2 anatase powder (p.a Merck), phenol red (p.a Merck), food-grade chitosan powder, 2% acetic acid (p.a Merck), epichlorohydrin (p.a Merck), 0.1% EDTA (p.a Merck), HCl (p.a Merck), NaOH (p.a Merck), ethanol (p.a Merck), and distilled water.

2.2. Methods

2.2.1. Manufacture of photocatalytic reactors

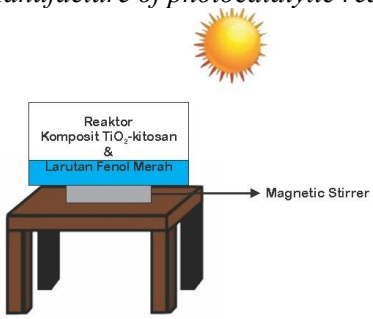

Figure 1. Arrangement of the Photocatalytic Reactor.

The reactor casing was built according to the dimensions of the waste reactor. The waste reactor was made of glass with a size of 25 cm × 10 cm. A glass tank was prepared to hold the dye wastewater. The tank was placed in an open area exposed to sunlight. A magnetic stirrer was placed inside the tank to prevent photocatalyst sedimentation. Figure 1 shows the arrangement of the photocatalysis reactor.

2.2.2. Synthesis of TiO_2–Chitosan Composite

The synthesis method of the TiO_2–chitosan composite used for degrading phenol red dye was adapted from the method proposed by Zhao et al. (2012). A total of 0.5 grams of chitosan powder and a specific amount of TiO_2

were dissolved in 20 mL of 2% acetic acid. The amount of TiO_2 was varied to observe the effect of the chitosan-to-TiO_2 ratio on the photocatalytic efficiency of the resulting TiO_2–chitosan composite. The mixture was continuously stirred for 45 minutes, followed by the addition of 1 mL of epichlorohydrin. Stirring continued for 5 hours at 30°C. The mixture was then dropped into a 0.25 M NaOH solution using a dropper to form beads.

The beads were left in the solution for 12 hours and then rinsed with distilled water. The TiO_2–chitosan beads were placed into an Erlenmeyer flask containing 100 mL of 0.1% EDTA solution and stirred at 30°C for 4 hours. The beads were then washed again with distilled water and subsequently stirred in 50 mL of 0.05 M NaOH solution at 30°C for 2 hours. Afterward, the TiO_2–chitosan beads were rinsed with distilled water and dried at 60°C. The resulting TiO_2–chitosan beads were characterized using SEM (Scanning Electron Microscope). The synthesis of the TiO_2–chitosan composite was repeated with varying TiO_2-to-chitosan ratios to determine the optimal composition. The TiO_2–chitosan ratios tested were 1:10, 2:10, and 5:10 (grams TiO_2: grams chitosan). The same procedure was also carried out using chitosan beads (without the addition of TiO_2).

2.2.3. Effect of Irradiation Time on the Reduction of Phenol Red Concentration

A total of 250 mL of 25 ppm phenol red solution was placed into the reactor, followed by the addition of 5 grams of beads. The mixture was continuously stirred at a speed of 400 rpm (Garg, 2015) while being irradiated in the reactor for 6 hours. At time intervals of 0, 20, 40, 60, 80, 100, 120, 140, 160, 180, 200, 220, 240, 260, 300, 320, 340, and 360 minutes, 5 mL samples of the solution were taken, and their absorbance was measured using a UV-Vis spectrophotometer at the maximum wavelength of phenol red.

2.2.4. Determination of the Optimum Dose of TiO_2–Chitosan

A total of 100 mL of 25 ppm phenol red solution was placed into the reactor, followed by the addition of varying amounts of TiO_2–chitosan composite. The composite-to-sample ratios used were 0.5:100, 1:100, 2:100, and 5:100 (grams of composite: volume of sample in mL). The mixture was continuously stirred at a speed of 400 rpm during irradiation (Garg, 2015). After reaching the optimum contact time, the remaining phenol red concentration in the sample was determined by measuring its absorbance at the maximum wavelength using a UV-Vis spectrophotometer. The same procedure was performed on 100 mL of the sample without TiO_2 addition as a negative control.

2.2.5. FTIR Analysis (Fourier Transform Infrared Spectrophotometer)

The obtained beads were analyzed using a Fourier Transform Infrared Spectrophotometer (FTIR). The beads were prepared using the KBr-press method, and spectra were recorded in the wavenumber range of 4000–400 cm^{-1}. This analysis aimed to identify the functional groups of both chitosan powder and chitosan beads by observing the absorption peaks of the functional groups (Kurniasih et al., 2016).

2.2.6. Data Analysis

The results of the TiO_2–chitosan study were obtained in the form of numerical data, including the optimum degradation time and the optimum dose of the TiO_2–chitosan composite in the degradation of phenol red. The data were organized using tabulation and graphs. The results were compared between irradiation using UV light and sunlight. The standard curve analysis and maximum wavelength determination of phenol red were performed using a UV-Vis spectrophotometer based on the Lambert-Beer law. FTIR spectroscopy was used to analyze the functional groups present in the TiO_2–chitosan composite based on the obtained spectra. The surface morphology of the TiO_2–chitosan composite was characterized using SEM.

3. RESULTS AND DISCUSSION

3.1. Synthesis of TiO_2–Chitosan Composite

The TiO_2–chitosan composite was prepared by dissolving TiO_2 and chitosan in 20 mL of 2% acetic acid, followed by stirring for 45 minutes. Then, 1 mL of epichlorohydrin was added, which acts as a crosslinking agent for chitosan. The mixture was stirred again for 5 hours until a thick, milky-white solution was obtained. This mixture was then converted into beads by dropping it into a 0.25 M NaOH solution. The formed beads were washed to remove residual NaOH and subsequently dried.

3.2 Functional Group Analysis of TiO_2–Chitosan Composite

To identify the functional groups, present in chitosan powder and the TiO_2–chitosan composite, Fourier Transform Infrared (FTIR) spectrophotometry analysis was conducted. The FTIR spectra of chitosan powder and TiO_2–chitosan composite is shown in Figure 2. The figure displays the transmittance values of the chitosan beads and TiO_2–chitosan composite as a function of the wavenumber.

A significant difference can be observed in the absorption patterns of the TiO_2–chitosan composite. Compared to the spectrum of unmodified chitosan, the TiO_2–chitosan composite exhibits a sharp absorption peak at around 3300 cm^{-1}, which indicates the stretching vibration of the –OH group. The broadening and shift of the –OH band are due to overlapping with the –NH group from amines. A sharp absorption peak is also observed at 1638 cm^{-1}, which is a characteristic peak of secondary amide (C=O) bonds. This absorption corresponds to the N–H stretching vibration of amides (Dompeipen, 2017). Another significant difference between the IR spectra of chitosan powder and the TiO_2–chitosan composite is the absorption observed in the wavenumber region around 650 cm^{-1}. As reported by Saravanan et al. (2018), the presence of absorption in this region indicates the incorporation of TiO_2 within the chitosan matrix.

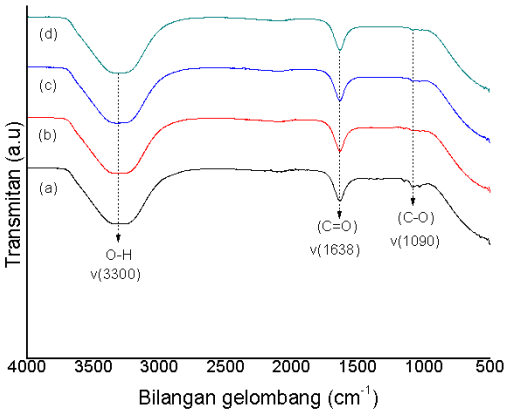

Figure 2. FTIR spectra of (a) Chitosan beads, (b) TiO_2–Chitosan composite 1:10, (c) TiO_2–Chitosan composite 2:10, and (d) TiO_2–Chitosan composite 5:10.

3.3. Morphological Analysis of TiO_2–Chitosan Composite

SEM analysis was conducted to observe the morphology of the composite on a microscopic scale. In this study, SEM analysis was performed on unmodified chitosan powder and TiO_2–chitosan composites. The SEM results of chitosan powder and TiO_2–chitosan composites with the three different TiO_2-to-chitosan ratios are shown in Figure 3.

Based on morphology at Figure 3(a), it can be observed that the surface of unmodified chitosan powder appears very rough. A different surface morphology is shown in Figure 3(b), which depicts the TiO_2–chitosan composite with a 1:10 ratio. In this image, the chitosan surface appears smoother, with white spots indicating TiO_2 particles attached to the chitosan surface. Figure 3(c) presents the SEM analysis of the TiO_2–chitosan composite with a 2:10 TiO_2-to-chitosan ratio, where a greater number of TiO_2 particles can be seen adhering

to the chitosan surface. The bright spots are more evenly distributed across the chitosan surface. Figure 3(d) shows the SEM result of the TiO_2–chitosan composite with a 5:10 ratio. A noticeable difference compared to other composites is observed, where TiO_2 particles on the chitosan surface tend to undergo agglomeration or clumping in certain areas.

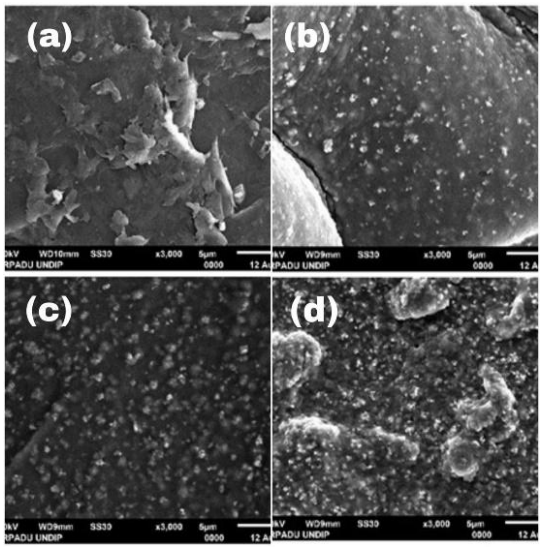

Figure 3. SEM analysis results (3000× magnification) of samples: (a) chitosan powder, (b) TiO_2–chitosan composite 1:10, (c) TiO_2–chitosan composite 2:10, and (d) TiO_2–chitosan composite 5:10.

3.4. Effect of Irradiation Time on the Reduction of Phenol Red Concentration

To study the effect of irradiation time on the reduction of phenol red concentration, TiO_2–chitosan composite was added to a phenol red solution with an initial concentration of 25 ppm at a ratio of 2:100 (g/mL). The solution and composite were exposed to sunlight for 6 hours, and the concentration of phenol red in the sample was analyzed every 20 minutes. The changes in phenol red concentration for each measurement over the observation period are presented in Figures 4, 5, 6, and 7.

Figure 4 shows that at the end of the observation period, after 6 hours of irradiation, the final concentration of phenol red was 16.386 ppm, corresponding to a reduction of 33.964% from the initial concentration. During the observation period, the concentration of phenol red fluctuated, indicating that the adsorption equilibrium of phenol red on chitosan had not yet been reached. Consequently, some of the phenol red that had been adsorbed was desorbed back into the solution.

Figure 5 shows that at the end of the observation period, after 6 hours of irradiation, the final concentration of phenol red was 18.207 ppm, representing a reduction of 23.775% from the initial concentration.

Figure 6 shows that at the end of the observation period, after 6 hours of irradiation, the final concentration of phenol red was 20.993 ppm, representing a reduction of 30.339% from the initial concentration.

Figure 7 shows that at the end of the observation period, after 6 hours of irradiation, the final concentration of phenol red was 21.707 ppm, representing a reduction of 10.988% from the initial concentration.

The effect of irradiation time was observed over a 6-hour period. Based on the pattern of phenol red concentration changes in the solution, the reduction of phenol red concentration occurred at an optimum rate during the first 20 minutes. This can be seen from the significant decrease in phenol red concentration within the initial 20 minutes. After the first 20 minutes and up to the end of the observation period, the phenol red concentration continued to decrease, but the reduction rate was no longer as high as that observed in the initial 20 minutes.

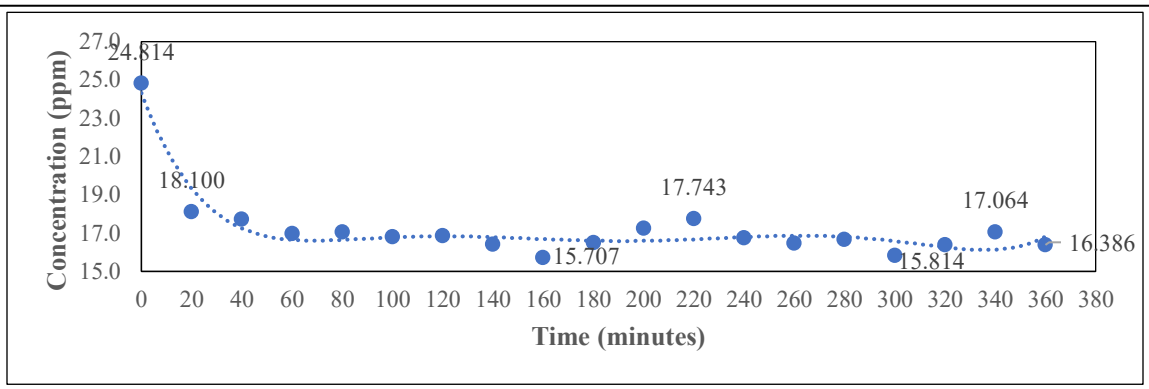

Figure 4. Effect of Irradiation Time (6 Hours) on the Reduction of Phenol Red Concentration in the Photocatalysis Process Using Chitosan Beads.

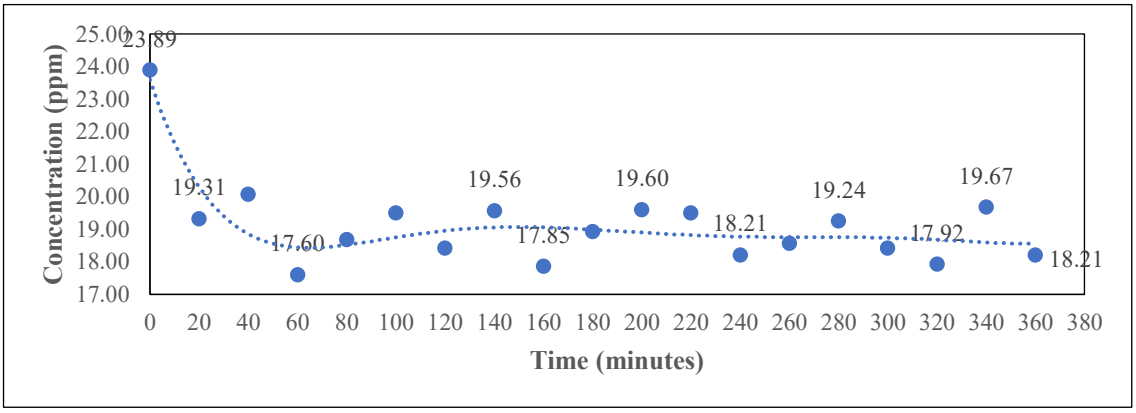

Figure 5. Effect of Irradiation Time (6 Hours) on the Reduction of Phenol Red Concentration in the Photocatalysis Process Using TiO_2–Chitosan Beads (1:10 Ratio)

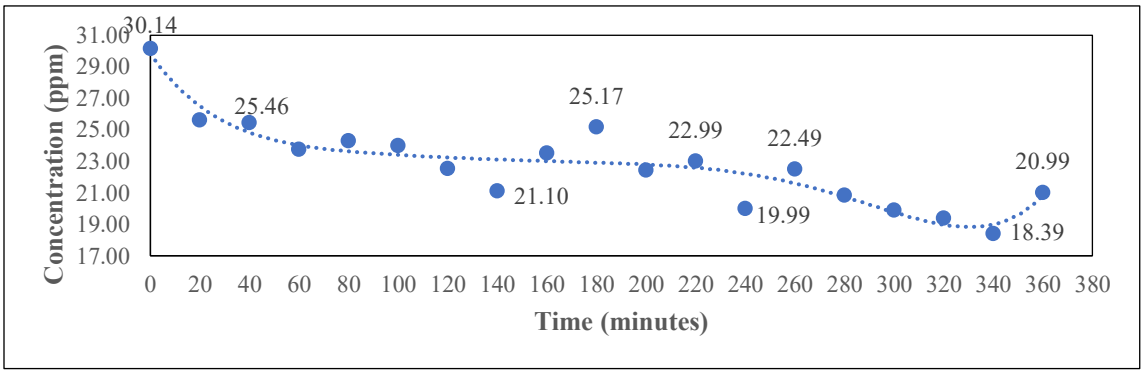

Figure 6. Effect of Irradiation Time (6 Hours) on the Reduction of Phenol Red Concentration in the Photocatalysis Process Using TiO_2–Chitosan Beads (2:10 Ratio)

When the sample was treated using TiO_2–chitosan composite beads, the reduction in phenol red concentration was estimated to occur through two processes: adsorption by chitosan and photocatalytic degradation catalyzed by TiO_2. However, the decrease in phenol red concentration observed with the TiO_2–chitosan composite was smaller compared to that with pure chitosan beads.

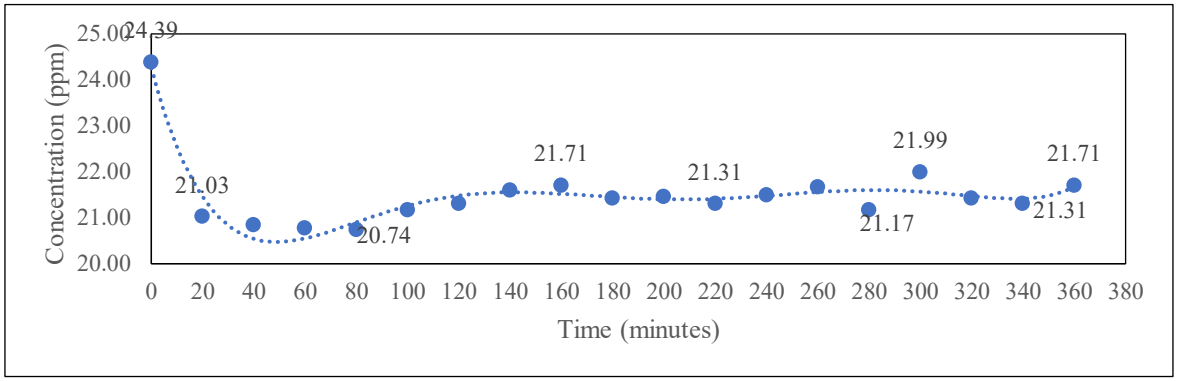

Figure 7. Effect of Irradiation Time (6 Hours) on the Reduction of Phenol Red Concentration in the Photocatalysis Process Using TiO_2–Chitosan Beads (5:10 Ratio)

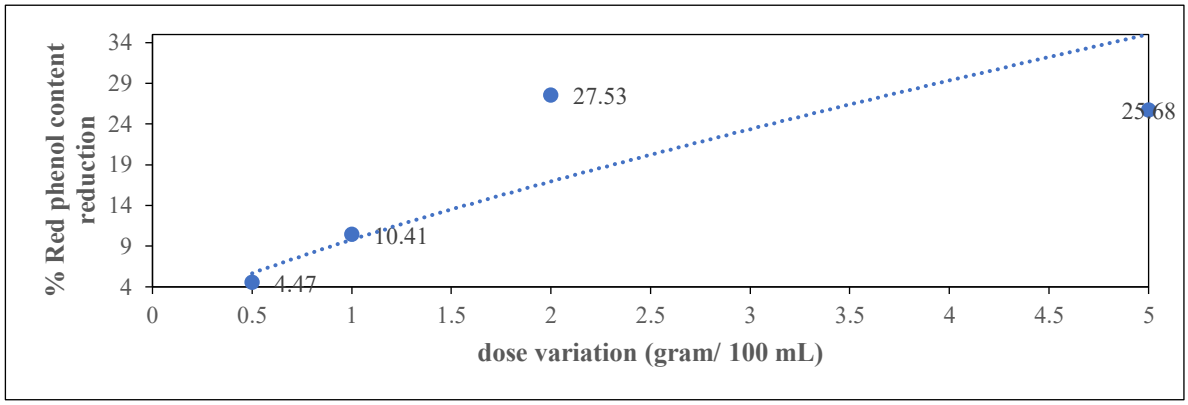

Figure 8. Results of Optimum Dose Determination using Chitosan Beads

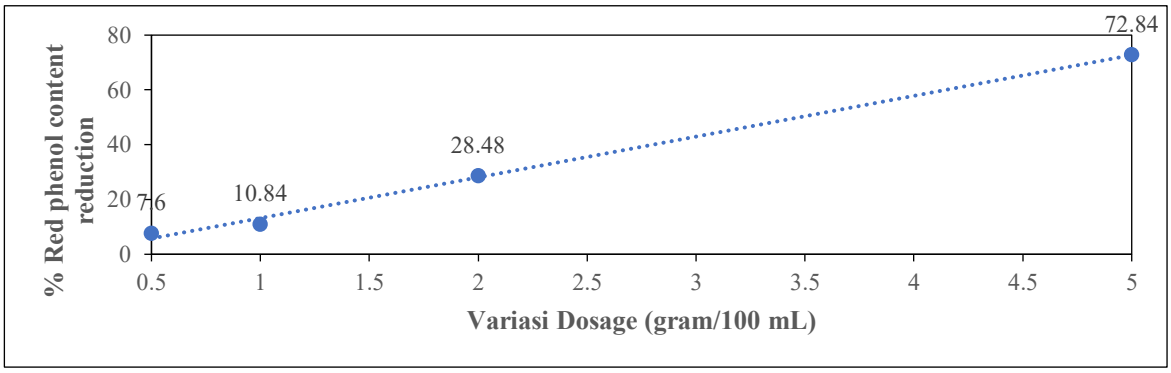

Figure 9. Optimum Dose Degtermination using TiO_2 Chitosan Beads with a 5:10 Ratio

This result indicates that the performance of chitosan in adsorbing phenol red, as well as the photocatalytic activity of TiO_2 in degrading phenol red, was not optimal. This is because the amine groups in chitosan, which play a crucial role in interacting with phenol red, are partially bonded to TiO_2 in the composite. TiO_2 bound to chitosan can also react with other TiO_2 particles dissolved in water (Saputro et al., 2016). Additionally, the decrease in the effectiveness of chitosan is also attributed to the use of epichlorohydrin, which forms covalent bonds with the –OH groups in chitosan (Gunawan et al., 2017).

3.5. Optimum Dose for Phenol Red Degradation

The purpose of determining the optimum dose of TiO_2–chitosan in the photochemical process of phenol red degradation is to identify the most effective amount of TiO_2–chitosan for achieving maximum degradation. In this study, the determination of the optimum TiO_2–chitosan dose was conducted by varying the ratio of TiO_2–chitosan to sample volume, namely 0.5:100, 1:100, 2:100, and 5:100 (grams/mL). In this degradation process, two types of beads were used: chitosan beads and composite beads with a TiO_2–chitosan ratio of 5:10 (grams:grams). Based on Figure 8, the optimum dose was obtained at a composition of 2:100 (g/mL), where the percentage reduction of phenol red concentration reached 27.53% from the initial concentration.

Based on Figure 9, the optimum dose was obtained at a 5:100 (g/mL) dosage variation, resulting in a 72.84% reduction of phenol red concentration. Figure 9 shows that the higher the TiO_2 ratio in the composite, the greater the percentage of phenol red degradation. This is because an increased amount of TiO_2 in the composite leads to the formation of more holes. These holes, formed during the excitation process, react with surrounding water molecules to produce highly reactive hydroxyl radicals. These hydroxyl radicals are extremely reactive and capable of degrading organic compounds effectively.

4. CONCLUSIONS

The conclusions of this study are as follows: The optimum TiO_2–chitosan ratio in the composite is 5:10. The optimum dose of the TiO_2–chitosan composite for photochemical degradation of 25 ppm phenol red is 5:100 (g/mL), achieving a reduction percentage of 72.84%. Furthermore, the longer the irradiation time (up to 6 hours) in the photocatalysis process using the TiO_2–chitosan composite, the greater the percentage of phenol red degraded through photochemical reactions.

ACKNOWLEDGMENT

The authors would like to express their gratitude to the Faculty of Mathematics and Natural Sciences (FMIPA), Universitas Lambung Mangkurat (ULM), for funding this research through the 2019 DIPA PNBP FMIPA. Sincere thanks are also extended to the academic supervisors, examiners, and all individuals who have provided support, knowledge, constructive criticism, and suggestions, enabling the completion of this research.

LIST OF REFERENCES

Aranas, I., Harris, R.., Heras, A., (2010), Chitosan Amphiphilic Derivatives. Chemistry and Applications, Current Organic Chemistry 14, 308-330.

Chiou, C.-H., Wu, C.-Y. & Juang, R.-S. (2008) 'Influence of operating parameters on photocatalytic degradation of phenol in UV/TiO_2 process', *Chemical Engineering Journal,* 139(2), pp. 322-329.

Dompeipen, E. J. (2017). Isolasi dan identifikasi kitin dan kitosan dari kulit udang Windu (Penaeus monodon) dengan spektroskopi inframerah. *Majalah Biam*, *13*(1), 31-41.

Febriyani, A. C., Hastuti, R., & Haris, A. (2012). Kajian Metode Elektrofotokatalisis, Elektrolisis dan Fotokatalisis pada Dekolorisasi Larutan Zat Warna Remazol Brilliant Orange 3R yang Mengandung Ion Logam Cu2+. *Jurnal Kimia Sains dan Aplikasi*, *15*(1), 7-12.

Garg, A., Mainrai, M., Bulasara, V.K. & Barman, S., (2015). Experimental Investigation on Adsorption of Amido black 10B dye onto zeolite synthesized

from fly ash. *Chemical Engineering Communications*, *202*(1), pp.123-130.

Gunawan, R., Shofiyani, A., & Zaharah, T. A. (2017). Pengaruh Penambahan Karbon Aktif Terhadap Sifat Permeabilitas Membran Komposit Kitosan Terikat Silang Epiklorohidrin. *Jurnal Kimia Khatulistiwa*, *7*(1).

Hashimoto, K., Irie, H. & Fujishima, A. (2005) 'TiO_2 photocatalysis: a historical overview and future prospects', *Japanese journal of applied physics,* 44(12R), pp. 8269.

Kurniasih, M., Riapanitra, A., & Rohadi, A. (2016). Adsorpsi rhodamin B dengan adsorben kitosan serbuk dan beads kitosan. *Sains & Matematika*, *2*(2).

Mittal, A., Kaur, D., Malviya, A., Mittal, J., & Gupta, V. K. (2009). Adsorption studies on the removal of coloring agent phenol red from wastewater using waste materials as adsorbents. *Journal of Colloid and Interface Science*, *337*(2), 345-354.

Saputro, A. N. C., Mulyani, B., Nurhayati, N. D., & Kurniawan, Y. (2016). Uji Kinerja Fotodegradasi Kain Terlapisi Komposit Nanosized Chitosan/TiO2 Terhadap Zat Warna Rhodamine B. *Jurnal Kimia Valensi*, *2*(1), 45-54.

Saravanan, R., Aviles, J., Gracia, F., Mosquera, E. & Gupta, V. K. (2018) 'Crystallinity and lowering band gap induced visible light photocatalytic activity of TiO2/CS (Chitosan) nanocomposites', *International journal of biological macromolecules,* 109, pp. 1239-1245.

Zhao, X., Xiao, G., Zhang, X., Su, H. & Tan, T., (2012). The Effect of Ni 2+ and Cu 2+ on the Photocatalytic Degradation of Dyes by the Chitosan–TiO_2 Complex. *Applied biochemistry and biotechnology*, *168*(1), pp.183-197.

JURNAL ILMIAH BERKALA SAINS DAN TERAPAN KIMIA

Jurnal Ilmiah Berkala: Sains dan Terapan Kimia
Vol. 19 No. 2, Juli 2025

Study on the Effect of Chitosan Concentration on the Synthesis of Epichlorohydrin Crosslinked Charcoal-Chitosan Composite on Its Ability to Adsorb Naphthol Blue Black Dye

Kajian Pengaruh Konsentrasi Kitosan Pada Sintesis Komposit Arang-Kitosan Terikat-Silang Epiklorohidrin Terhadap Kemampuannya Dalam Mengadsorpsi Zat Warna *Naphthol Blue Black*

Salma Nur Aida [1] Dahlena Ariyani [1]* Umi Baroroh Lili Utami [1] Dyah Ayu Pramoda Wardani [1] Ahmad Budi Junaidi [1]

Department of Chemistry, Faculty of Mathematics and Natural Sciences, Lambung Mangkurat University, Banjarbaru 70714, Indonesia

Email: *dariyani@ulm.ac.id*

ABSTRACT

The synthesis of a charcoal–chitosan composite crosslinked with epichlorohydrin (ACCE) as an adsorbent for naphthol blue black dye was carried out to improve the suboptimal adsorption capacity of activated charcoal. This study aims to characterize the functional groups and water content of the ACCE composite and to investigate the effect of chitosan concentration on its adsorption performance. The ACCE composites were prepared by mixing activated charcoal with chitosan solutions at various ratios, followed by crosslinking with epichlorohydrin. The effects of contact time, pH, and initial dye concentration on the adsorption capacity of naphthol blue black were examined. FTIR analysis of the ACCE composite confirmed the interaction between activated charcoal and chitosan crosslinked by epichlorohydrin, indicated by the appearance of a peak at 2377 cm^{-1}, attributed to N–H bending. The adsorption study showed that equilibrium was achieved at 30 minutes. The pH effect revealed that the highest adsorption percentage was obtained at neutral pH, with the AC8CE2 composite achieving 10.26 mg/g, likely due to enhanced chitosan stability by the crosslinker. Furthermore, increasing the initial dye concentration resulted in higher adsorption capacities, with AC8CE2, AC8CE4, AC8CE6, and AC8CE8 composites reaching 32.86 mg/g, 29.49 mg/g, 26.06 mg/g, and 28.08 mg/g, respectively.

Keywords: Adsorption, activated charcoal, chitosan, epichlorohydrin, naphthol blue black.

ABSTRAK

Sintesis komposit arang-kitosan terikat-silang epiklorohidrin (ACCE) sebagai adsorben zat warna *naphthol blue black* telah dilakukan karena kapasitas adsorpsi dari arang aktif kurang maksimal. Penelitian ini bertujuan untuk mengetahui karakteristik gugus fungsi dan kadar air komposit ACCE, serta mendapatkan data pengaruh konsentrasi kitosan terhadap kemampuan adsorpsinya di dalam komposit ACCE sebagai adsorben zat warna *naphthol blue black.* Komposit ACCE terdiri dari campuran arang aktif dan larutan kitosan dari berbagai variasi rasio yang diikat silang menggunakan

epiklorohidrin kemudian dianalisis pengaruh waktu kontak, pH, dan konsentrasi awal terhadap kemampuan adsorpsi zat warna *naphthol blue black.* Hasil karakterisasi spektra FTIR pada komposit ACCE menunjukkan bahwa telah terjadi interaksi antara arang aktif dan kitosan terikat-silang epiklorohidrin, hal tersebut dibuktikan dengan bilangan gelombang 2377 cm^{-1} yang muncul pada spektrum komposit ACCE yang diidentifikasikan sebagai N-H tekuk. Pengaruh waktu kontak dengan variasi menunjukkan bahwa waktu kesetimbangan tercapai pada waktu 30 menit. Pengaruh pH optimum menunjukkan bahwa persentase adsorpsi paling tinggi terjadi pada pH netral yaitu pada komposit AC8CE2 mencapai 10,26 mg/g, hal tersebut dikarenakan adanya pengikat-silang dapat meningkatkan stabilitas kitosan. Pengaruh konsentrasi awal terhadap kemampuan adsorpsi menunjukkan semakin meningkatnya konsentrasi awal, maka akan meningkatkan kemampuan adsorpsi dari zat warna *naphthol blue black* yaitu pada komposit AC8CE2 mencapai 32,86 mg/g, komposit AC8CE4 mencapai 29,49 mg/g, komposit AC8CE6 mencapai 26,06 mg/g dan komposit AC8CE8 mencapai 28,08 mg/g.

Keywords: Adsorpsi, arang aktif, kitosan, epiklorohidrin, *naphthol blue black*.

Received: 17 May 2025 ; **Accepted**: 26 July 2025: **Available online**: 30 July 2025

1. INTRODUCTION

The increasing use of dyes in various industries, such as food and textiles, has led to significant environmental problems. Discarded dye waste is particularly concerning as it affects the aesthetic quality of the environment. Moreover, the presence of dyes can inhibit the penetration of sunlight, thereby reducing photosynthetic activity, especially for aquatic organisms living at the bottom of water bodies. Dyes can also become toxic when they interact with metals and chlorine present in the water. This issue is further compounded by the fact that most dyes are resistant to biological degradation, making it necessary to remove or reduce them from aquatic environments. (Fransina, 2008).

Dyes widely used in the textile industry often belong to the azo dye group, which is the largest class of synthetic dyes due to their stability during the dyeing process. One example of an azo dye is naphthol blue black. This dye is commonly used to color fabrics such as wool, nylon, silk, and batik. Naphthol blue black dye is difficult to degrade, especially when its concentration exceeds the permissible limits. According to the Regulation of the Minister of Environment and Forestry of the Republic of Indonesia Number P.16/MENLHK/SETJEN/KUM.1/4/2019, the quality standards for textile wastewater set the maximum allowable BOD at 60 mg/L and COD at 150 mg/L. Moreover, naphthol blue black is non-biodegradable and possesses carcinogenic and mutagenic properties that negatively impact the environment. Therefore, wastewater containing naphthol blue black must be properly treated before being discharged into water bodies (Kusumawardani & Purbasari, 2022).

Several methods have been developed to address environmental pollution caused by liquid organic compounds from textile industry dyes, including coagulation, filtration, and adsorption. Among these, adsorption is recognized as one of the most effective methods for removing color from dye-contaminated wastewater. Various adsorbent materials can be used for this purpose, such as activated carbon and chitosan (Fitriansyah et al., 2021). The first step in achieving an effective adsorption process is selecting an adsorbent with high selectivity and capacity that can also be reused (Fransina, 2008).

Activated charcoal has long been used as an adsorbent for dyes. Research by Hamu et al. (2019) on the use of activated charcoal derived from hazelnut shells (Aleurites moluccana L.

Willd) for naphthol blue black dye removal reported an adsorption capacity of 3.58 mg/g. Activated charcoal possesses a good pore structure and high surface area; however, it lacks abundant functional groups, resulting in predominantly physical adsorption. To enhance its adsorption performance, chitosan can be added to activated charcoal, as chitosan is rich in functional groups such as amine and hydroxyl groups that promote chemical adsorption. Nevertheless, chitosan is unstable under acidic conditions, making it necessary to investigate the synthesis of charcoal–chitosan composites in this study.

Chitosan is a natural polymer with abundant availability; however, it has the drawback of being unstable in acidic conditions, making crosslinking necessary. Chitosan can be crosslinked using agents such as glutaraldehyde (GLA), epichlorohydrin (ECH), ethylene glycol diglycidyl ether (EDGE), and tripolyphosphate (TPP)(Ariyani et al., 2018). The use of epichlorohydrin (ECH) as a crosslinker offers the advantage of targeting the hydroxyl groups of chitosan while preserving its amine groups, which are essential for effective dye adsorption. This crosslinking process is expected to enhance the stability of chitosan in acidic conditions and improve its adsorption capacity (Mardila et al., 2014). Additionally, crosslinking with ECH increases the chemical stability of chitosan, making it insoluble in concentrated acids (pH 1) and bases (Madjid et al., 2018). Based on the above description, this study investigates the effect of chitosan concentration on the synthesis of an epichlorohydrin-crosslinked charcoal–chitosan composite as an adsorbent for naphthol blue black dye.

2. MATERIALS AND METHODS

2.1. Materials

The tools used in this research included an analytical balance (Ohaus), oven (Thermologic), and various glassware (Pyrex), such as beakers, volumetric flasks, Erlenmeyer flasks, volumetric pipettes, dropper pipettes, iron spoons, glass spoons, test tubes, glass funnels, and reagent bottles. Other equipment included a magnetic stirrer, pH meter (DrGray), spray bottle, and analytical instruments such as a Fourier Transform Infrared (FTIR) Spectrophotometer (Platinum ATR Bruker) and a UV-Vis Spectrophotometer (Genesys 10V).

The materials used in this study included chitosan powder derived from shrimp shells (GMP) (moisture content ≤12.0%, ash content ≤1.0%, protein content ≤1.0%, DAC ≥70%), activated charcoal (p.a. Merck, particle size <100 mesh), acetic acid (100%) (E. Merck), sodium hydroxide (NaOH) crystals, concentrated hydrochloric acid (HCl), naphthol blue black dye, epichlorohydrin (analytical grade, Fluka), pH paper, aluminum foil, distilled water, and Whatman No. 42 filter paper.

2.2. Preparation of epichlorohydrin crosslinked charcoal-chitosan composite

In this study, charcoal–chitosan composites were prepared with chitosan solution concentrations of 1%, 2%, 3%, and 4%. To prepare a 1% chitosan solution, 2 g of chitosan powder was weighed using an Ohaus analytical balance, dissolved in 200 mL of 2% acetic acid solution, and stirred until homogeneous. Subsequently, 8 g of activated charcoal was added to the solution and stirred thoroughly. A mixture of 0.5 M NaOH and 1% epichlorohydrin (200 mL) was then added slowly while stirring vigorously. The resulting chitosan gel was allowed to stand for 24 hours, filtered using Whatman No. 42 filter paper, rinsed with distilled water, and dried in an oven at 60°C until a constant weight was achieved. The same procedure was repeated to prepare charcoal–chitosan composites with chitosan concentrations of 2%, 3%, and 4%, each using 200 mL of acetic acid, 8 g of activated charcoal, and 200 mL of the NaOH–epichlorohydrin mixture. The resulting epichlorohydrin-crosslinked charcoal–chitosan composites were labeled as AC8CE2, AC8CE4, AC8CE6, and AC8CE8, corresponding to 1%, 2%, 3%, and 4% chitosan solutions, respectively. Each composite was then analyzed for functional group characteristics using an FTIR spectrophotometer and for moisture content using the gravimetric method.

2.3. Moisture content test

The weight of the empty container and filter paper was recorded prior to use. A total of 0.5 g of the AC8CE2 composite was weighed using an analytical balance and placed into an Erlenmeyer flask. The composite was dried at 105 °C until a constant weight was achieved, then cooled in a desiccator and weighed again to determine the change in mass. The same procedure was carried out for the AC8CE4, AC8CE6, and AC8CE8 composites.

2.4. Preparation of naphthol blue black standard curve

Naphthol blue black solutions with concentrations of 3, 4, 5, 6, and 7 ppm were prepared by diluting a 50-ppm stock solution of naphthol blue black. The absorbance of each solution was then measured using a UV-Vis spectrophotometer at the maximum wavelength of 618 nm.

2.5. Effect of contact time on the ability of epichlorohydrin crosslinked charcoal-chitosan composite to adsorb naphthol blue black dye

A 50 ppm naphthol blue black solution was prepared by diluting a 1000 ppm standard solution using a 5 mL volumetric pipette and transferring it into a 100 mL volumetric flask, followed by dilution to the mark with distilled water. A total of 0.5 g of the dry AC8CE2 composite was weighed using an analytical balance and placed in an Erlenmeyer flask. Then, 100 mL of the 50 ppm naphthol blue black solution was added to the flask. The mixture was shaken using a shaker at 120 rpm for 5, 15, 30, 60, and 120 minutes. After shaking, the composite and filtrate were separated using Whatman No. 42 filter paper, and the filtrate's absorbance was measured with a UV-Vis spectrophotometer. The same procedure was repeated for the AC8CE4, AC8CE6, and AC8CE8 composites.

2.6. Effect of pH on the ability of epichlorohydrin crosslinked charcoal-chitosan composite to adsorb naphthol blue black dye

Acidic, neutral, and basic variations of the 50 ppm naphthol blue black solution were prepared by adjusting the pH using 2% HCl solution to lower the pH and 0.5 M NaOH solution to increase it. A total of 0.5 g of the dry AC8CE2 composite was weighed using an analytical balance and placed in an Erlenmeyer flask, followed by the addition of 100 mL of the 50 ppm naphthol blue black solution. The mixture was shaken using a shaker at 120 rpm for the optimum contact time. The composite and filtrate were then separated using Whatman No. 42 filter paper, and the filtrate's absorbance was measured using a UV-Vis spectrophotometer. The same procedure was repeated for the AC8CE4, AC8CE6, and AC8CE8 composites.

2.7. Effect of initial concentration of epichlorohydrin crosslinked charcoal-chitosan on naphthol blue black

Naphthol blue black solutions with concentrations of 10, 20, 30, and 40 ppm were prepared by diluting a 1000 ppm standard solution and adjusting the pH to the optimum value. A total of 0.1 g of the AC8CE2 composite was weighed using an analytical balance and placed into an Erlenmeyer flask, followed by the addition of 100 mL of the prepared naphthol blue black solution. The mixture was shaken using a shaker at 120 rpm for the optimum contact time. The composite and filtrate were then separated using Whatman No. 42 filter paper, and the absorbance of the filtrate was measured using a UV-Vis spectrophotometer. The same procedure was repeated for the AC8CE4, AC8CE6, and AC8CE8 composites.

2.8. Data Analysis

The water content of the composites was analysed using the gravimetric method. This involved weighing the empty filter paper and then weighing the filter paper containing the ACCE composites after the preparation process. The percentage of water content was calculated using the following equation:

$$Moisture\ content\ (\%) = \frac{initial\ weight\ (g) - final\ weight\ \ (g)}{Initial\ weight\ (g)} \times 100\%$$

The dye adsorption process by the ACCE composites was analyzed using a UV-Vis spectrophotometer at a wavelength of 618 nm.

The absorbance values obtained were converted into concentration values using Microsoft Excel. The percentage (%) of dye adsorbed by the ACCE composite was calculated using the following equation:

$$C_a = C_o - C_e$$

Where,

Ca : Concentration of absorbed substance (ppm)

Co : Initial concentration of solution (ppm)

Ce : Residual dye concentration (ppm)

$$(\%)\ \text{Adsorption} = \frac{Ca}{Co} \text{x } 100\%$$

The data obtained from parameters such as contact time and pH were presented as graphs showing the relationship between the percentage of dye adsorption and contact time, as well as the relationship between the percentage of dye adsorption and pH.

Determination of the amount of adsorbate adsorbed:

The amount of adsorbate adsorbed per unit mass of adsorbent (qeqe, mg/g) was calculated using the following equation:

$$q_e = \frac{Ca\left(\frac{v}{1000}\right)}{m}$$

where,

qe : amount of adsorbed substance (mg/g)

v : volume (mL)

m : mass of adsorbent (g)

3. RESULTS AND DISCUSSION

The initial stage of this study involved the synthesis of a charcoal–chitosan composite crosslinked with epichlorohydrin (ACCE). The purpose of creating this composite was to combine the advantages of both materials—charcoal and chitosan—to enhance dye adsorption efficiency. The composite was prepared by mixing activated charcoal with chitosan, followed by crosslinking with epichlorohydrin. A 2% acetic acid solution was used to dissolve the chitosan, as chitosan is a cationic polymer that is insoluble in water but easily soluble in organic acids. Acetic acid facilitates the dissolution of chitosan into a homogeneous solution (Purwaningsih et al., 2020).

Activated charcoal in powder form was mixed with a chitosan solution and stirred until homogeneous, followed by the slow addition of a mixture of 0.5 M NaOH solution and 1% epichlorohydrin to form an epichlorohydrin-crosslinked charcoal–chitosan gel. This process produces a composite with high adsorption capacity, making it suitable for applications such as dye removal from water or heavy metal adsorption. The formation of crosslinks in chitosan improves its properties, including reduced solubility in water and organic solvents, as well as enhanced mechanical strength of the resulting particles (Sulistyawati et al., 2020). The formation of the epichlorohydrin-crosslinked charcoal–chitosan composite occurs due to interactions between the hydroxyl and carboxyl groups on activated charcoal and the hydroxyl and amine groups on chitosan, as illustrated in Figure 1.

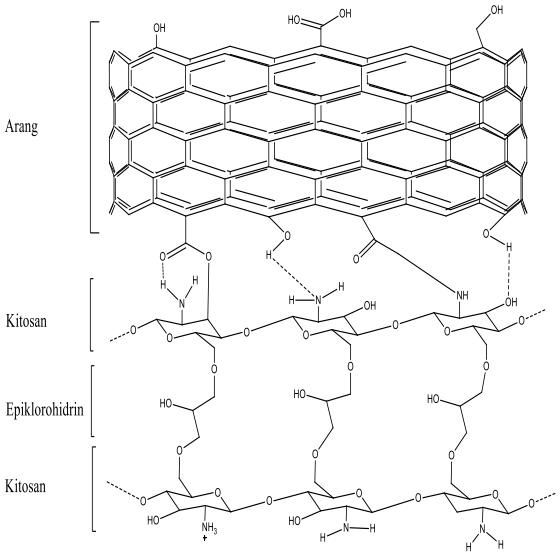

Figure 1. Interaction of activated charcoal, chitosan, and epichlorohydrin

Chitosan dissolves readily in solutions with pH values below 6 and is stable around pH 7, which means it can easily be released or degraded in conditions of pH ≤ 6 when used as an adsorbent. The addition of crosslinking agents can enhance the stability of chitosan under acidic conditions, making it more effective for adsorption applications (Utami *et al*., 2015). Epichlorohydrin crosslinking of chitosan in an alkaline medium occurs through

the formation of covalent bonds between the carbon atoms of epichlorohydrin and the hydroxyl groups of chitosan. This process involves the breaking of the epoxide ring of epichlorohydrin and the release of chlorine atoms, as the reactive sites of epichlorohydrin are located within its epoxide and chlorine groups (Nisfayati et al., 2017). According to Gunawan et al. (2017), crosslinked charcoal–chitosan composites exhibit greater stability compared to non-crosslinked composites. This increased stability is due to the ability of crosslinkers to enhance the mechanical properties of the material, although this may slightly reduce the adsorption capacity.

3.1. Characterization of functional groups of epichlorohydrin crosslinked charcoal-chitosan composites

FTIR spectrophotometric analysis of the composite was carried out to identify the functional group characteristics of the epichlorohydrin-crosslinked charcoal–chitosan (ACCE) composite. The peaks in the FTIR spectrum indicate interactions between charcoal, chitosan, and epichlorohydrin, which are often reflected by shifts in the wave numbers of specific functional groups. The FTIR characterization results of chitosan, activated charcoal, and the ACCE composites are presented in Figure 2.

Based on Figure 6, the infrared spectra display the characteristic peaks of activated charcoal, chitosan, and the ACCE composite, which combines the features of both materials. The functional groups identified from the infrared spectra of activated charcoal, chitosan, and the ACCE composite are summarized in Table 1.

The FTIR spectrum of activated charcoal shows a peak at 2071 cm^{-1}, which corresponds to C=C alkene bonds. The presence of these bonds may result from the activation process of the charcoal and is also observed in the ACCE composite. This suggests that the presence of double bonds in carbon compounds can indicate a high level of purity. Additionally, an absorption band at 1563 cm^{-1} in activated charcoal is identified as an aromatic C=C stretching vibration. This functional group is also present in the ACCE composite, with a slight shift to 1543 cm^{-1}. Such a shift in wave number indicates interactions between the components and suggests that both activated charcoal and the ACCE composite have the potential to adsorb carbon dioxide.

An absorption band at 2377 cm^{-1} was observed in the ACCE composite, which was identified as N–H bending.

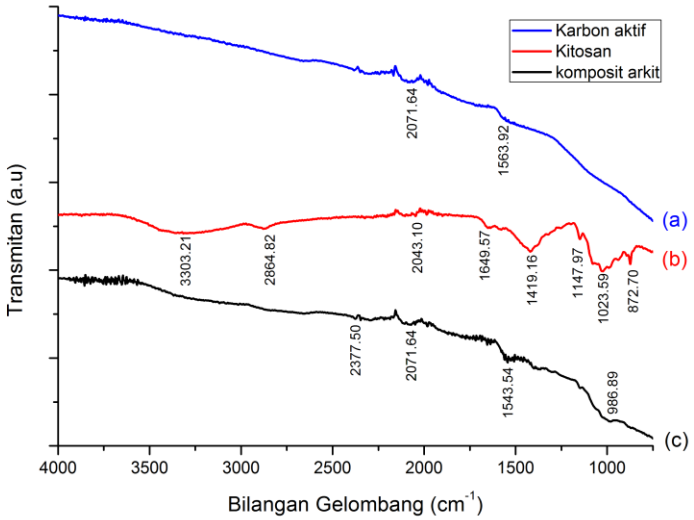

Figure 2. IR spectra of activated charcoal (a), chitosan (b), and ACCE composite (c)

Table 1. Identification of functional groups of activated carbon, chitosan, and chitosan-carbon

Active Charcoal (cm^{-1})	Chitosan (cm^{-1})	ACCE composite (cm^{-1})	Wavelength (cm^{-1})	Functional Group	Reference
	3303		3500-3200	−NH/−OH that is hydrogen bonded	(Sastrohamidjojo, 19
	2864		2850-2950	Unsaturated or Aromatic Alkanes	(Sastrohamidjojo, 20
		2377	2337	N−H bending	(Zaenudin, 2014).
2071	2043	2071	2100-2260	C=C Alkene	(Eso *et al*., 2021).
	1649		1850-1630	Carbonyl (C=O)	(Sastrohamidjojo, 19
1563		1543	1640-1540	C=C aromatic	(Sartika *et al*., 2014).
	1419	1421	1465-1370	C−H bending vibrations	(Andiani *et al*., 2022)
	1147				
	1023		1075-1020	C−O−C Symmetric stretching vibrations	(Sastrohamidjojo, 19
		986	986	C−H bending vibrations	(Silverstein, Bassler,
	872		909-666	Symmetrical stretch N−H	(Sastrohamidjojo, 19

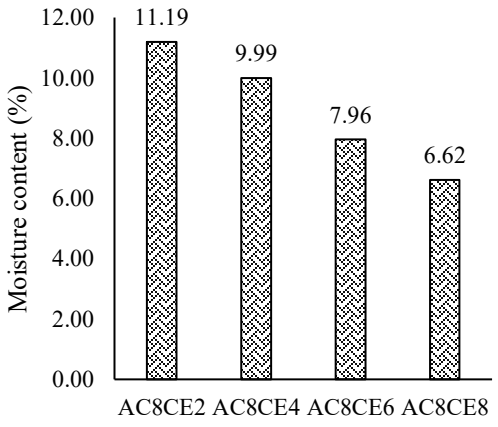

Figure 3. Graph of percentage moisture content at various ratios of epichlorohydrin crosslinked charcoal-chitosan composites

This peak was absent in the spectrum of activated charcoal prior to activation with dyes, indicating the formation of crosslinking between activated charcoal and chitosan.

Additionally, an absorption band at 3303 cm^{-1} appeared in the spectrum of chitosan, attributed to –NH and –OH stretching vibrations involved in hydrogen bonding. This peak suggests the formation of bonds between the hydrocarbon groups in chitosan and epichlorohydrin.

3.2. Moisture Content

The moisture content of the composite was determined using the gravimetric method. This analysis aims to measure the water content by calculating the difference between the initial and final weights of the sample after drying. The gravimetric method involves weighing the sample before and after drying to a constant weight. The effect of chitosan solution concentration on the moisture content of the composite is presented in Figure 3.

Based on the graph in Figure 3, it can be observed that as the concentration of the chitosan solution increases, the moisture content of the composite decreases. This occurs because the pores of the charcoal

become denser with the addition of more chitosan, reducing the amount of water retained within the composite. A lower moisture content enhances the adsorption capacity of the ACCE composite for naphthol blue black dye, as less residual water remains to block the pores (Mudaim & Hidayat, 2021).

percentage of naphthol blue black adsorption by the composites is presented in Figure 4.

Based on the curve in Figure 4, the percentage of naphthol blue black adsorption increases with increasing contact time. The results indicate that the adsorption process reaches equilibrium at an optimum contact time of 30 minutes.

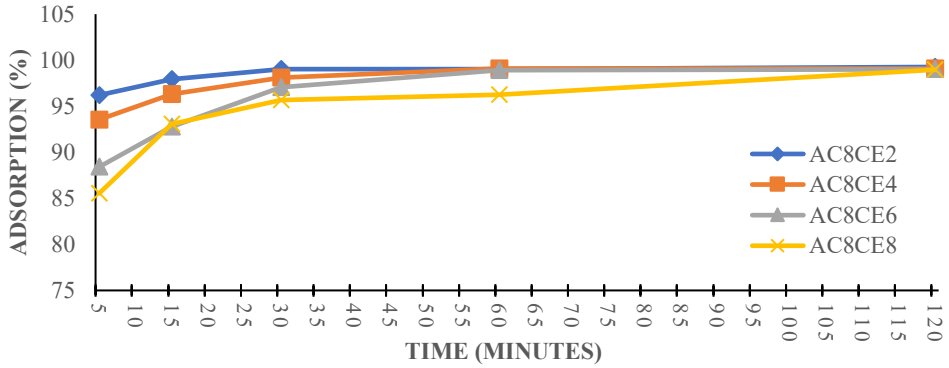

Figure 4. Relationship curve between contact time and adsorption percentage of naphthol blue

The results of this study show that the moisture content of the composites ranges from 6.62% to 11.19%, which complies with the SNI 06-3730-1995 standard that specifies a maximum moisture content of 15% for powder-form adsorbents.

3.3. Effect of contact time on the adsorption ability of naphthol blue black

The determination of adsorption contacts time aims to identify the duration required for the adsorbent and adsorbate to reach adsorption equilibrium. Adsorption equilibrium is achieved when the rate of particle adsorption onto the adsorbent surface equals the rate of desorption (Wulandari *et al*., 2021). Each composite was contacted with a 50 ppm naphthol blue black solution at varying contact times of 5, 15, 30, 60, and 120 minutes, while being shaken at a stirring rate of 120 rpm. The residual concentration of naphthol blue black in the solution after contact with the composite was measured using a UV-Vis spectrophotometer at a wavelength of 618 nm. The adsorption percentage was determined based on the reduction in naphthol blue black concentration before and after adsorption. The relationship between contact time and the

The graph in Figure 4 also shows that higher chitosan concentrations lead to a slower attainment of adsorption equilibrium and a lower overall adsorption capacity. This is likely due to the predominance of physical adsorption, which depends on the pore structure and surface area of the composite. The addition of excess chitosan can block the pores of the activated charcoal, reducing the available surface area for adsorption. At the initial stage of the adsorption process, the pores of the activated charcoal are still open and unoccupied by naphthol blue black dye particles, providing a greater opportunity for the dye molecules to penetrate and be adsorbed. Consequently, the adsorption capacity increases sharply at the beginning until it stabilizes upon reaching the equilibrium condition (Syafrianda *et al*., 2017). After the equilibrium time is reached, the curve becomes linear, indicating that the adsorbed dye is not easily released despite collisions between the composite and water during stirring. According to Sulistyawati (2008), adsorption capacity increases proportionally with time up to a certain point, after which it stabilizes or decreases once equilibrium is achieved.

3.4. Effect of optimum pH

Determination of pH is an important variable in the adsorption process, as it influences the surface charge of both the adsorbent and the adsorbate in the solution. The presence of hydroxyl ions (OH^-) and hydrogen ions (H^+) during the pH adjustment process affects the electrostatic interactions between the composite and the naphthol blue black dye molecules (Hayu *et al*., 2021). In this study, the pH of the naphthol blue black dye solution was varied to represent acidic (pH 3.55), neutral (pH 7.01), and alkaline (pH 9.91) conditions. After contact with the composite, the remaining concentration of naphthol blue black in the solution was measured using a UV-Vis spectrophotometer at a wavelength of 618 nm. The results of this experiment are presented in Figure 5.

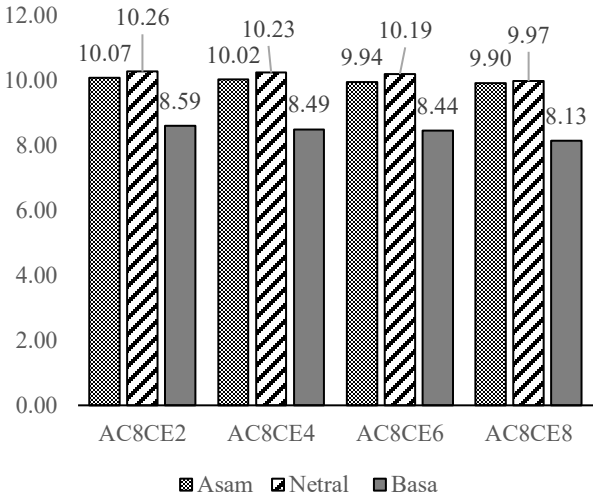

Figure 5. Graph of the effect of pH on the adsorption ability of naphthol blue black on charcoal-chitosan composites.

The graph in Figure 5 indicates that increasing the chitosan concentration in the composite affects its adsorption capacity. The results show that the highest dye adsorption occurs at neutral pH. This is because, under neutral conditions, the amino groups of chitosan can exist in both deprotonated ($-NH_2$) and protonated ($-NH_3^+$) forms, enabling strong electrostatic interactions with the sulfonate groups of the naphthol blue black dye. As a result, the adsorption interaction is maximized at neutral pH compared to acidic or alkaline conditions (Siswati *et al.*, 2014).

The interactions between the dye, activated charcoal, chitosan, and epichlorohydrin are illustrated in Figure 6.

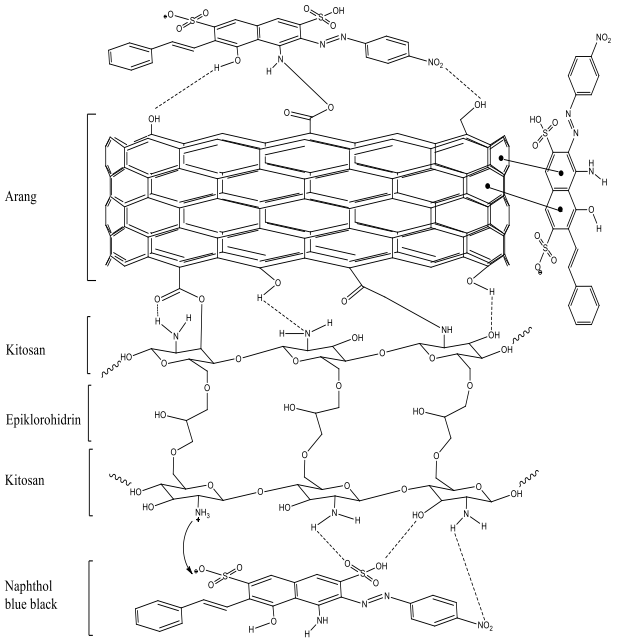

Figure 6. Interaction between ACCE composite and naphthol blue black dye

Under neutral conditions, some of the amine groups ($-NH_2$) in chitosan interact with H^+ ions from the environment, becoming protonated to form $-NH_3^+$ groups. These positively charged groups can then interact with the anionic sulfonate groups of the dye, forming ionic bonds or strong electrostatic interactions that enhance the adsorption process (Pembayun & Rahmayanti, 2020). At acidic pH, the high concentration of H^+ ions in the solution leads to interactions with the hydrophilic groups on the composite surface. This excessive protonation reduces the availability of active adsorption sites, thereby inhibiting the interaction between the composite and naphthol blue black dye. In contrast, at alkaline pH, the naphthol blue black dye tends to interact with Na^+ ions from the base to form salts. Additionally, the presence of OH^- ions can create partial negative charges on the dye molecules,

weakening the electrostatic interactions with the adsorbent (Baunsele & Missa, 2020).

3.5. Determination of adsorption capacity

The determination of the initial dye concentration was conducted to identify the optimum conditions under which the composite exhibits maximum adsorption capacity. Adsorption experiments of naphthol blue black on charcoal–chitosan composites were performed with initial dye concentrations of 10, 20, 30, and 40 ppm at neutral pH and an equilibrium time of 30 minutes.

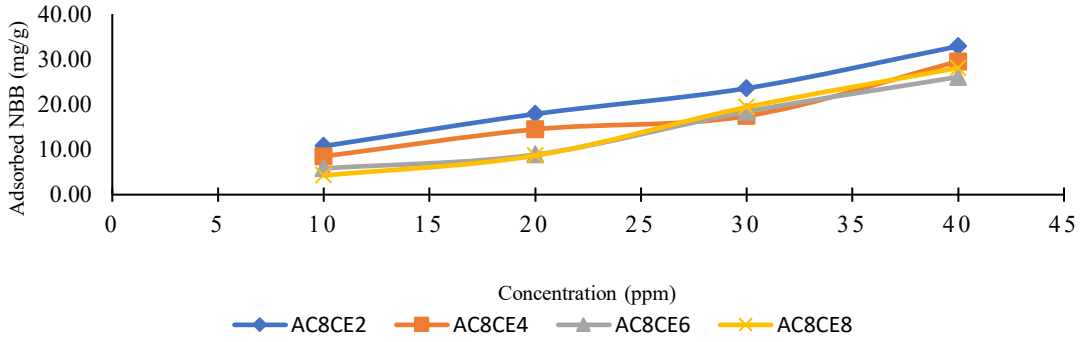

Figure 7. Relationship curve of initial concentration and adsorption ability at equilibrium state (mg/g)

The results, expressed as the amount of naphthol blue black adsorbed per gram of composite (mg/g), are presented in Figure 7, which illustrates the relationship between the initial dye concentration and the adsorption capacity. Based on the graph in Figure 7, the results of this study show that the initial concentration of naphthol blue black dye significantly influences the amount of dye adsorbed by the ACCE composites. As the initial concentration increases, the adsorption capacity also increases. This is because adsorbents possess a finite number of active sites, and each site has an equal probability of binding with adsorbate molecules. If the active sites are not saturated, an increase in the adsorbate concentration results in a greater amount of adsorbate bound to the surface (Utami et al., 2009). In this study, the highest adsorption capacity was achieved at an initial concentration of 40 ppm, with AC8CE2 reaching 32.86 mg/g, AC8CE4 reaching 29.49 mg/g, AC8CE6 reaching 26.06 mg/g, and AC8CE8 reaching 28.08 mg/g. However, at higher concentrations, the adsorption ability of the ACCE composites begins to decrease due to surface saturation, which is likely caused by the increased chitosan content reducing the surface area and pore availability of the composite. Zein *et al.* (2019) in Hayu *et al*. (2021) explains that the adsorption capacity increases with increasing dye concentration due to stronger electrostatic interactions between the active sites on the adsorbent surface and the dye molecules.

4. CONCLUSIONS

The conclusion of this research is:

1. The FTIR spectra of the ACCE composites confirm interactions between activated charcoal and chitosan, as indicated by the appearance of a peak at 2377 cm^{-1}, which is identified as N–H bending. Increasing the concentration of chitosan results in a lower water content within the ACCE composites.
2. The percentage adsorption of naphthol blue black dye by the ACCE composites increased with contact time (5–120 minutes) and reached equilibrium at the optimum time of 30 minutes. A higher chitosan concentration slowed the time required to reach equilibrium and reduced the adsorption capacity.
3. The adsorption of naphthol blue black dye by ACCE composites is influenced by pH, with the optimum adsorption occurring at neutral pH. At this condition, the AC8CE2 composite achieved an adsorption

capacity of 10.26 mg/g. The concentration of chitosan in the composite preparation significantly affects adsorption performance in the presence of crosslinkers.

4. The adsorption capacity of epichlorohydrin-crosslinked charcoal–chitosan composites toward naphthol blue black dye is also affected by the initial solution concentration. At an initial concentration of 40 ppm, the adsorption capacities were 32.86 mg/g for AC8CE2, 29.49 mg/g for AC8CE4, 26.06 mg/g for AC8CE6, and 28.08 mg/g for AC8CE8.

ACKNOWLEDGMENT

Thanks are conveyed to the BELMAWA Directorate of the Ministry of Education, Culture, Research, and Technology for funding research on the student creativity program (PKM) in the field of research and Sekolah Tinggi Analis Kimia Cilegon for funding and providing laboratory facilities

LIST OF REFERENCES

A. Fitriansyah, H.A, E. 2021. Karakterisasi Adsorben Karbon Aktif dari Sabut Pinang (*Areca catechu*) terhadap Kapasitas Adsorpsi Zat Warna Indigosol Blue 04-B. *Jurnal Pendidikan Dan Ilmu Kimia.*, **5(1):** 42–54.

Andiani, B. Y., Riyanto, C. A., & Martono, Y. 2022. Characterization of Cassava (*Manihot esculenta Crantz*) Peel Activated Carbon based on Impregnation Ratio and Activation Temperature. *Stannum : Jurnal Sains Dan Terapan Kimia.*, **4(1)**: 19–26. https://doi.org/10.33019/jstk.v4i1.2533

Ardianto, R., & Amalia, R. 2023. Optimasi Proses Deasetilasi Kitin menjadi Kitosan dari Selongsong Maggot menggunakan RSM. *Metana: Media Komunikasi Rekayasa Proses dan Teknologi Tepat Guna.,* **19(1):** 1–12.

Ariyani, D., Cahaya, N., & Mujiyanti, D. R. 2018. Pengaruh pH dan Waktu Kontak Terhadap Adsorpsi Logam Zn (II) pada Komposit Arang Eceng Gondok Termodifikasi Kitosan-Epiklorohidrin. *Jurnal Kimia Valensi : Jurnal Penelitian dan Pengembangan Ilmu Kimia.,* **4(2):** 85–92.

Baunsele, A. B., & Missa, H. 2020. Kajian Kinetika Adsorpsi Metilen Biru Menggunakan Adsorben Sabut Kelapa. *Akta Kimindo*., **5(2):** 76–85.

Chandrasekaran, M., Kim, K. D., & Chun, S. C. 2020. Antibacterial Activity of Chitosan Nanoparticles : A Review. *Processes.*, **8(1173):** 1–21.

Dewi, R., Azhari, A., & Nofriadi, I. 2021. Aktivasi Karbon dari Kulit Pinang dengan Menggunakan Aktivator Kimia KOH. *Jurnal Teknologi Kimia Unimal*, **9(2)**: 12. https://doi.org/10.29103/jtku.v9i2.3351

Eso, R., Luvi, & Ririn. 2021. Efek Variasi Konsentrasi Zat Aktivator H_3PO_4 Terhadap Morfologi Permukaan dan Gugus Fungsi Karbon Aktif Cangkang Kemiri. *Gravitasi*., **20(1):** 19–23.

Fransina, E. G. 2008. Studi Kinetika Adsorpsi Biru Metilena pada Kitin dan Kitosan. *J. Sains MIPA.,* **13(3)**: 171–176.

Gunawan, R., Shofiyani, A., & Zaharah, T. A. 2017. Pengaruh Penambahan Karbon Aktif Terhadap Sifat Permeabilitas Membran Komposit Kitosan Terikat-Silang Epiklorohidrin *JKK*., **7(1):** 1–9.

Hamu, G. V., Gauru, I., & Kadang, L. 2019. Pemanfaatan Arang Aktif Tempurung

Kemiri (*Aleurites moluccana L. Willd*) Sebagai Adsorben Zat Warna *Naphthol*. *Chem. Notes*., **1(2):** 12–23.

Hasanah, N. 2023. Skripsi Kinerja Butiran Kitosan Terikat-Silang Epiklorohidrin (ECH) dan Glutaraldehid (GLA) Terhadap Adsorpsi *Remazol Yellow Fg.*

Hayu, L. D. R., Nasra, E., Azhar, M., & Etika, S. B. 2021. Adsorpsi Zat Warna *Methylene Blue* Menggunakan Karbon Aktif dari Kulit Durian (*Durio zibethinus Murr.*). *Chemistry Journal of Universitas Negeri Padang*., **10(2):** 8–13.

Kusumawardani, R., & Purbasari, A. 2022. Synthesis and Performance Evaluation of Magnetized Modified Coal Fly Ash as Adsorbent for Naphthol Blue Black Dye Removal from Synthetic Dye Wastewater. *TEKNIK*., **43(3):** 222–227. https://doi.org/10.14710/teknik.v43i3.48337

Madjid, A. D. R., Nitsae M., & Sabarudin A. 2018. Perbandingan Butiran Kitosan dengan Pengikat Silang Epiklorohidrin (ECH) dan Glutaraldehid (GLA): Karakterisasi dan Kemampuan Adsorpsi Timbal (Pb). *Alchemy : journal of chemistry*., **6(1):** 29-37.

Mau, Y. P., Suyasa1, I. W. B., & Suprihatin, I. E. 2018. Biodegradasi Zat Warna *Naphthol Blue Black* Menggunakan Biosistem Horizontal. *Jurnal Kimia.*, 201. https://doi.org/10.24843/jchem.2018.v12.i02.p17

Miri, N. S. S., & Narimo. 2022. Review : Kajian Persamaan Isoterm Langmuir dan Freundlich pada Adsorpsi Logam Berat Fe (II) dengan Zeolit dan Karbon Aktif dari Biomassa. *Jurnal Kimia Dan Rekayasa.*, **2(2):** 58–71. http://kireka.setiabudi.ac.id

Mudaim, S., & Hidayat, S. 2021. Analisis Proksimat Karbon Kulit Kemiri (*Aleurites Moluccana*) Dengan Variasi Suhu Karbonisasi. *Jurnal Ilmu Dan Inovasi Fisika.*, **5(2):** 157–163.

Nitsae, M., Solle, H. R. L., Martinus, S. M., & Emola, I. J. 2021. Studi Adsorpsi Methylene Blue Terhadap Arang Aktif Tempurung Lontar (*Borassus Flabellifer L.*) Asal Nusa Tenggara Timur. *Jurnal Kimia Riset.*, **6(1):** 46. https://doi.org/10.20473/jkr.v6i1.24525

Pembayun, S. Retno W., & Rahmayanti, M. 2020. Efektivitas Biji Asam Jawa Sebagai Koagulan Alam*i. Jurnal Sains dan Teknologi*., **9(2):** 162–169.

Purwaningsih, D. Y., Anisa, D., & Putri, A. D. O. 2020. Kitosan Sebagai Koagulan untuk Removal Warna pada Limbah Cair Industri Pangan. *Seminar Nasional Sanis Dan Teknologi Terapan VII.I*, 541–546.

Rahmi, Lubis, S., Adlim, M., Lelifajri, Zahra, M. A., & Fathanah, H. 2023. *Pemanfaatan Selulosa dari Bahan Alam Pada Pembuatan Komposit Kitosan.* Syiah Kuala University Press, Banda Aceh

Ramadhani, L. F., Nurjannah, I. M., Yulistiani, R., & Saputro, E. A. 2020. Review : Teknologi Aktivasi Fisika pada Pembuatan Karbon Aktif dari Limbah Tempurung Kelapa. *Jurnal Teknik Kimia.,* **26(2)**: 42–53.

Safitri, G. A. 2016. Skripsi Pengaruh Variasi Komposisi PVA/Kitosan Terhadap Perilaku Membran Komposit PVA/Kitosan/Grafin Oksida yang Terikat Silang Trisodium Sitrat.

Sartika, N. D., Gumbira-Sa'id, E., Machfud, Sunarti, T. C., & Pari, G. 2014. Kajian Pembuatan Arang Aktif Berbahan Baku Bagas Tebu Melalui Kombinasi Proses Karbonisasi Hidrotermal dan Aktivasi Kimia. *Jurnal Teknologi Industri Pertanian.*, **24(2):** 157–165.

Sastrohamidjojo. 1992. *Spektroskofi Inframerah*. Liberty, Yogyakarta

Sastrohamidjojo. 2001. *Kimia Dasar*. Gadjah Mada University Press, Yogyakarta

Shofa. 2012. Pembuatan Karbon Aktif Berbahan Baku Ampas Tebu Dengan Aktivasi Kalium Hidroksida. *Universitas Indonesia.*, 1–84.

Silverstein, Bassler, & Morril. 1986. *Penyidikan Spektrometrik Senyawa Organik*. Erlangga, Jakarta.

Suhartati, T. 2017. *Dasar-dasar Spektrofotometer UV-Vis dan Spektrofotometer Massa untuk Penentuan Senyawa Organik*. AURA, Bandar Lampung.

Sulistyawati, E., Nandari, W. W., Nurchasanah, A. R., & Dewi, K. K. 2020. Kinetika Adsorpsi Mikrokapsul Kitosan Taut Silang Kalium Persulfat Terhadap Zat Warna *Methyl Orange*. *Jurnal Rekayasa Proses.*, **14(1):** 47–59. https://doi.org/10.22146/jrekpros.50634

Syafrianda, I., Yenie, E., & Daud, S. 2017. Pengaruh Waktu Kontak dan Laju Pengadukan Terhadap Adsorpsi Zat Warna pada Air Gambut Menggunakan Adsorben Limbah *Biosolid Land Application* Industri Minyak Kelapa Sawit. *Jom FTEKNIK.*, **4(2):** 1–6.

Utami, L., & Rohman, T. 2009. Adsopsi Pb (II) oleh Kitosan Terlapiskan pada Arang Aktif Cangkang Kelapa Sawit. *J Sains Mipa.,* **15(2):** 89–99.

Utami, U. B. L., Mujiyanti, D. R., & Normilawati. 2015. Kajian Adsorpsi Cd (II) oleh Arang Apu-Apu Termodifikasi Kitosan-Glutaraldehida. *Sains Dan Terapan Kimia.*, **9(2):** 12–22.

Wulandari, R., Dewi, W. N., F, M. F. R., Afni, R. A., & Dwijayanti, A. 2021. Efektivitas Adsorben Bonggol Jagung Terhadap Kadar Klorin Pada Air PDAM. *Chemtech*, **7(1):** 22–27.

Zaenudin, M. 2014. Skripsi Studi Pendahuluan Interaksi Ekstrak Campuran Daun Saga (*Abrus Precatorius L.*), Gambir (*Uncaria Gambir R.*), dan Kapur Sirih (CaO), dengan Metode Spektroskopi UV-Sinar Tampak dan Inframerah